Charge and mass exchange in ^{56}Fe-induced reactions at 8.3 MeV/nucleon

H. Breuer

Department of Physics and Astronomy, University of Maryland, College Park, Maryland 20742

A. C. Mignerey

Department of Chemistry, University of Maryland, College Park, Maryland 20742

V. E. Viola

Department of Chemistry and Indiana University Cyclotron Facility, Indiana University,
Bloomington, Indiana 47405

K. L. Wolf*

Argonne National Laboratory, Argonne, Illinois 60439

J. R. Birkelund, D. Hilscher,† J. R. Huizenga, W. U. Schröder, and W. W. Wilcke

Department of Chemistry and Physics and Nuclear Structure Research Laboratory,
University of Rochester, Rochester, New York 14627

Projectilelike fragments from reactions of 465-MeV ^{56}Fe projectiles with targets of ^{56}Fe, ^{165}Ho, ^{209}Bi, and ^{238}U have been measured as a function of energy loss, and neutron and proton number. The mass and charge of each fragment were uniquely determined with discrete resolution. Data were analyzed as a function of energy loss by fitting a two-dimensional Gaussian function to the neutron-proton distributions. The fit parameters provide a convenient basis for comparison with theoretical predictions. In addition, centroids and variances derived from more detailed one-dimensional Gaussian fits to isobaric charge distributions are presented. Results are given for measured data as well as for the primary fragment distributions after correction for the dominant neutron evaporation. The centroid data show that in the asymmetric reactions proton transfer from projectile to target nucleus is preferred while the average fragment neutron number is largely preserved. This produces a charge equilibration process which is dependent on energy loss within the combined systems. The neutron and proton variances indicate an early dominant neutron flow followed by a constant relative neutron and proton exchange rate at energy losses above about 30 MeV. The degree of correlation of the neutron-proton distributions increases with energy loss and is found to be strongly related to the potential energy surface. Consistently observed negative correlation coefficients at low energy losses suggest the possible importance of processes other than particle exchange in the early stages of the interaction. Variances for constant N, Z, and A are found to saturate at energy losses and with magnitudes dependent on the target nucleus.

> NUCLEAR REACTIONS ^{56}Fe, ^{165}Ho, ^{209}Bi, ^{238}U + ^{56}Fe, E_{lab}=465 MeV; simultaneous energy, mass and charge determination for projectilelike fragments; parametrization in terms of two-dimensional Gaussian functions; neutron and proton distribution centroids, variances, and correlation coefficients; properties of charge equilibration and nucleon exchange.

I. INTRODUCTION

In the past most experimental studies of damped collisions between heavy target-projectile partners have involved the determination of the energy, charge, and angular distributions of the reaction products. For a more complete characterization of the energy dissipation and nucleon-exchange process it is highly desirable to obtain simultaneously the mass of the reaction products. Owing to the increased complexity of experiments that yield both mass and charge identification, only a few studies of this nature have been published[1-17] for reactions where both the projectile and target have mass numbers larger than 40.

Several of these studies have concentrated[1-7,18] on the properties of charge variances at fixed mass, $\sigma_Z^2(A)$. The experimental data published do not yet constitute a general basis for the understanding of this degree of freedom. Notably, whether or not the values for these variances saturate[1-5,18] at high energy losses or continue to increase[6,7] has not been conclusively determined. This question is important for an evaluation of the processes involved and limitations imposed on nucleon exchange along a path perpendicular to the potential-energy surface. These vari-

ances may also yield information about the importance of nonstatistical energy loss mechanisms.

A further focus of attention has been the process of charge equilibration[3−5,8−11,18−22] which is important if the projectile and target have different proton-to-neutron number ratios. Although the existence of this effect is well established, a detailed understanding of the mechanisms and time scales involved in this equilibration process depends on the availability of detailed and systematic data.

Simultaneous mass and charge data allow the determination of the correlation between neutron and proton fragment distributions. This correlation, for which only few data have been analyzed,[2,5,6,9−13,18] can yield detailed information about the relation between proton and neutron exchange. In addition, energy-loss processes other than statistical ones may be recognized by correlations which cannot be explained on a pure nucleon-exchange basis.

Theoretical calculations often require mass data for comparison if all nucleons are treated equally, or both proton and neutron number data if the charge asymmetry degree of freedom is included. A priori, the neutron number or mass number of fragments from damped collisions cannot be deduced from measured charge distributions.[9,16] Thus, it is of great importance to obtain a more complete experimental basis for the description of these processes. Also, simultaneous A and Z data permit theoretical investigations of heavy-ion reactions from new and, until recently, unprecedented perspectives.[23−33] Among these are the evaluation of mechanisms[4,7,23−26] based on quantal and statistical vibrations and calculations that include explicitly the Pauli principle[27,28] and specific forms of the level-density parameters.[29]

The goal of this study is to provide a systematic investigation of discrete nuclide distributions of projectilelike fragments as a function of energy loss and projectile-target mass asymmetry. The projectile was kept constant at ^{56}Fe, sufficiently heavy to be representative of a large class of heavy-ion projectiles. The targets varied from the symmetric ^{56}Fe nucleus to the mass-asymmetric targets ^{165}Ho, ^{209}Bi, and ^{238}U. Along with the increase in projectile-target mass asymmetry goes an increase in the projectile-target asymmetry of neutron excess. To keep as many variables fixed as possible, the laboratory energy of the projectile ^{56}Fe was 8.3 MeV/nucleon for all reactions studied. This energy corresponds to very similar amounts of energy available above the Coulomb barrier in the center-of-mass frame for each system: about 140 MeV. The determination of the dependence on incident projectile energy and mass will be important in the future to complete a comprehensive characterization of damped collisions in terms of mass, charge, and dissipated energy. Special attention should also be given to previous experimental studies involving the ^{56}Fe nucleus (Refs. 1, 2, 9, 10, 12, 16, 17, 21, 34−36, and data in Ref. 31), which provide a rather detailed picture of Fe-induced reactions.

This paper intends to provide a consistent set of high resolution data that can serve as a basis for comparison with theoretical calculations that yield explicit results for both neutron (or mass) and proton distributions of projec-

tilelike fragments (Refs. 3, 4, 12, 19, 20, 23, 24, 27−32, and 37−39). Thus, after having summarized in Sec. II the technical background for obtaining the data, the paper will concentrate in Sec. III on the description of different possible representations of these data and the intrinsic correlations between these presentations. Section IV compares the main results with similar experimental data published to date and some theoretical calculations of relevance to the subjects discussed. Section V summarizes the basic conclusions of the paper.

II. EXPERIMENTAL PROCEDURES AND DATA REDUCTION

In this section a brief summary of the experimental procedures and data reduction techniques is given. A more detailed discussion, including the equations used to transform the fit results and their uncertainties and to correct data for the effects of experimental resolution and binning (assignment of discrete channel numbers to continuous data), can be found in Ref. 16.

A. Experiments

The experiments were performed at the Lawrence Berkeley Laboratory SuperHILAC with ^{56}Fe beams of 465±5 MeV laboratory energy incident on 400- to 800-μg/cm^2 self-supporting monoisotopic ^{56}Fe, ^{165}Ho, ^{209}Bi, and ^{238}U targets. A ΔE-E solid state surface barrier detector telescope (ΔE detector: 50 mm^2 active area, 16 μm thick, 12 cm distance from the target; E detector: 300 mm^2 active area, > 60 μm thick) was used to determine the laboratory energy and to identify the charges Z of reaction fragments. A flight path of approximately 95 cm between ΔE and E detectors yielded time-of-flight information from which the mass A of each fragment could be determined, thus providing discrete nuclide A and Z information simultaneously. Electropolished circular apertures in front of both detectors defined solid angles of 2.0 msr for the ΔE detector and 0.2 msr for the E detector. The time-of-flight information was obtained with fast time pickoff units of the Sherman-Roddick design[40] which yielded a time resolution of better than 80 psec for elastically scattered ^{56}Fe ions.

Detection angles for projectilelike reaction products were chosen near the grazing angle of the respective projectile-target combination. Table I shows the laboratory detection angles as well as some reaction parameters[41] of the systems under investigation. For the Bi and U targets data were taken at two laboratory angles; the smaller one to obtain a sufficient cross section for the complete range of energy losses, E_L, and the larger angle to obtain good data at low E_L with little contamination due to slit-scattering[16] of elastically scattered ^{56}Fe particles. Approximately 200 000 to 500 000 inelastic events per angle were recorded. The slow variation of cross section with angle seen in Wilszyński plots[35,36] for these systems makes the variations in c.m. angle for different masses at fixed laboratory angle unimportant for the present study. At the highest energy losses, especially in the ^{238}U + ^{56}Fe reaction, nonorbiting and orbiting fragment distributions,

TABLE I. Entrance-channel properties and reaction parameters for the ^{56}Fe, ^{165}Ho, ^{209}Bi, and ^{238}U + ^{56}Fe reactions at a laboratory energy of 465 MeV. The Coulomb energy E_C, the quarter point angle in the laboratory system, $\theta_{1/4}^{lab}$, and the maximum angular momentum expected to lead to reactions l_{max}, are taken from Ref. 41.

	Z	N	N/Z	E_C (MeV)	$E_{c.m.} - E_C$ (MeV)	$\theta_{1/4}^{lab}$	θ_{exp}	l_{max} ($\hbar$)
^{56}Fe	26	30	1.154					
^{165}Ho	67	98	1.463					
^{209}Bi	83	126	1.518					
^{238}U	92	146	1.587					
^{56}Fe + ^{56}Fe	52	60	1.154	85	147	13°	8°	160
^{165}Ho + ^{56}Fe	93	128	1.376	189	158	33°	30°	235
^{209}Bi + ^{56}Fe	109	156	1.431	226	140	40°	34°,38°	236
^{238}U + ^{56}Fe	118	176	1.492	246	131	48°	40°,45°	234

which presumably represent different interaction times, may be present at energy losses above 150 MeV. The angles chosen minimize the orbiting fragment contribution.

B. Calibration of data

The channel numbers representing the energies recorded in ΔE and E detectors and the time of flight of each fragment were converted into the total laboratory energy, E_{lab}, the charge Z, and the mass A for each fragment. The energy calibration,[16] based on elastic scattering at angles where the elastic peak dominates as well as on a precision pulser normalized with alpha-particle sources, was estimated to be correct within 5 MeV and to better than 1% in energy differences (energy differences are important for the accuracy of the energy-loss scale). The energy resolution, including the spread in accelerator beam energy and straggling in the target, was approximately 5 MeV as observed from the width of the elastic peak. The resolution in charge and mass was typically 0.7 to 0.9 charge units and 0.7 atomic mass units for elastically scattered ^{56}Fe ions. The absolute calibration[16] for all Z and A with significant cross section was accurate within ±0.05 units at all E_L.

C. Total kinetic energy loss determination and estimates for particle evaporation

The total kinetic energy loss, E_L, determined in the center-of-mass (c.m.) system of the reaction partners is the total reaction Q value for a pair of fragments directly after the interaction and prior to deexcitation, mainly by particle emission. To obtain E_L, the c.m. energy of the detected fragments was determined with a two-body kinematical calculation that includes an estimate of the primary mass A', i.e., the mass before deexcitation by particle emission. Pure isotropic neutron emission and a division of the total excitation energy E_t^* ($E_t^* = E_L - Q_{gg}$) according to the primary masses of the reaction partners was assumed. The ground-state Q value Q_{gg} and the neutron separation energy S_n were taken into account for each event to calculate[16] A' and E_L.

For the excitation energies of projectilelike fragments E^* typical of the reaction discussed here ($E^* \lesssim 70$ MeV), the same number of nucleons are evaporated at a given E^*

in the first approximation, independently of the combination of emitted protons, neutrons, or alpha particles. Also, this procedure results in corrections of less than 16 MeV on the E_L scale as compared to a two-body kinematic calculation which neglects particle evaporation. Thus, any error on the E_L scale due to the assumption of pure neutron emission is small.

In contrast, the corrections required to estimate primary mass and charge distributions are more critical. No attempt was made to obtain the primary mass, charge, or neutron number distributions for the ^{56}Fe + ^{56}Fe reaction. This symmetric system, with high possible excitation energies in both reaction partners, was found to deexcite both by neutron and charged particle emission (Sec. III A *1*), thus making estimates about the primary A' and Z' highly model dependent. For the asymmetric reactions involving the ^{165}Ho, ^{209}Bi, and ^{238}U targets much less excitation energy is expected to be deposited in projectilelike fragments ($\lesssim 35$ MeV as compared to $\lesssim 70$ MeV for data obtained for the ^{56}Fe + ^{56}Fe system). More important, even the *observed* projectilelike fragments exhibit a high degree of neutron excess (Sec. III A *3*) and, consequently, low neutron binding energies. Both observations indicate that for the asymmetric reactions the primary fragments decay principally by neutron deexcitation[34] with average multiplicities of fewer than three neutrons. Thus, for the asymmetric reactions the corrections made to obtain primary fragment distributions are much better defined than for the Fe + Fe reaction.

In this paper, the measured mass of a fragment is represented by A, the calculated mass prior to deexcitation by A'. The corresponding neutron numbers of reaction products are defined by $N = A - Z$ and $N' = A' - Z$. Z always represents the measured charge. Measured data are usually shown in the figures as circles with error bars. In cases where the procedure to account for particle emission results in a good approximation to the primary data, the corrected values are represented in the figures by triangles without any indication of the uncertainty.

D. Possible effects of small-angle scattering in the ΔE detector

The ΔE detector represents a thick scattering source with respect to the reaction fragments. For a flight path

of 95 cm not all fragments detected in a given solid angle at the ΔE detector location will also be recorded in the same solid angle by the E detector. The average small angle scattering angle depends on the charge of the fragment and its energy[42]; thus the measured charge and mass distributions may become distorted.

To estimate the significance of this process, the experiment was simulated by a Monte Carlo program that included the experimental geometry and expressions taken from Belery et al.,[42] which are independent of the mass of the projectile. The program calculates the cross section, charge centroid, and charge variance of fragments originating from an initial Gaussian distribution with $\bar{Z}_i = 26$ and $\sigma_i^2 = 25$, and detected after passing through a 16.3 μm Si detector. In general, the centroid of the detected distribution is more strongly affected by small-angle scattering than is the variance. For instance, for fragments with $E_{lab} = 100$ MeV, the detected distribution was calculated to be a Gaussian with $\bar{Z}_f = 25.46 \pm 0.01$ and $\sigma_f^2 = 25.00 \pm 0.05$. The deviation between $\bar{Z}_i$ and $\bar{Z}_f$ scales with σ_i^2 and decreases rapidly with increasing E_{lab}. Above $E_{lab} = 250$ MeV the deviation in $\bar{Z}$ for $\sigma_z^2 = 25$, vanishes. A misalignment between ΔE and E detectors of less than $\pm 1.0°$ does not change $\bar{Z}_f$ or σ_f^2 significantly for $E_{lab} > 100$ MeV. The detection efficiency remains constant at the ratio of the solid angles of the E and ΔE detectors for a misalignment of up to $\pm 0.4°$ for $E_{lab} > 100$ MeV.

For all data presented here, the final laboratory energy was above 230 MeV and $\sigma_Z^2 \leq 25$. Thus, no corrections arising from small-angle scattering in the ΔE detector were considered to be necessary. The main reason for the insensitivity of the detected distribution to small-angle scattering is the (deliberately chosen) large difference in solid angle between ΔE and E detectors. This allows in-scattering to compensate nearly perfectly for any out-scattering, even if ΔE and E detectors are not perfectly aligned.

E. Generation of spectra

Examples of mass and charge spectra for all projectile-like fragments with $E_L > 30$ MeV detected in the ^{165}Ho + ^{56}Fe reaction at 30° are shown in Fig. 1. To obtain the properties of the mass and charge distributions, either one-dimensional (for mass or charge) or two-dimensional spectra were produced with gates on E_L having a width of 10 MeV (4 MeV for low E_L two-dimensional spectra). The E_L values quoted later represent the central value of this gate.

One-dimensional mass (charge) spectra were gated in addition by the charge (mass) with a width of ± 0.3 units. The remaining small contributions of cross sections from neighboring charges (masses) have been subtracted. The one-dimensional spectra discussed in this paper (figures showing examples may be found in Ref. 16) were generated with one channel (bin) per mass or charge unit.

Two-dimensional spectra do not require any gate in addition to the one imposed on E_L. These spectra were generated with a resolution of two channels per N and Z in the N-Z plane given directly by the experiment. The neu-

tron number N was calculated on an event-by-event basis with $N = A - Z$ or $N' = A' - Z$. Some of these two-dimensional N-versus-Z spectra are shown in Fig. 2 as contour diagrams. Properties of the mass distributions can be calculated from the fit parameters discussed in the next section.

F. Fit procedures

As is well known, the major part of the cross section for charge and mass spectra of damped products at a constant energy loss can usually be well represented by a Gaussian function with appropriate centroids $\bar{z}$ and variances σ_z^2 ($z = A$, A', Z, N, or N'). However, many of these spectra exhibit small tails in addition to the dominant Gaussian component. These can often be attributed to processes other than damped reactions (e.g., sequential fission of the target nucleus). The results of a Gaussian fit for $\bar{z}$ and σ_z^2 are much less dependent on the tails of the distributions and on the somewhat arbitrary judgment of the experimenter about the necessary fit limits,[16] than is a moment analysis for $\bar{z}$ and σ_z^2. Thus, for this work only Gaussian least-squares fits have been used to obtain the results.

It has also been found[2,16] that the two-dimensional distributions can be well represented, and thus parametrized, by a two-dimensional Gaussian function. This can be seen in Fig. 2, where the contour lines form nearly concentric ellipses. At high E_L for the ^{238}U + ^{56}Fe reaction, the con-
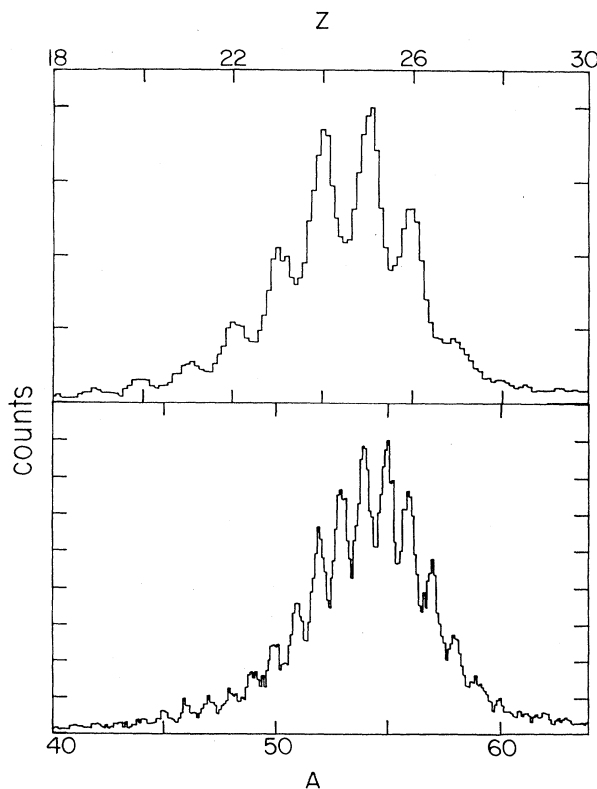

FIG. 1. Charge and mass spectra for damped products from the 465-MeV ^{165}Ho + ^{56}Fe reaction at 30°. These spectra contain all data recorded with $30 \leq E_L \leq 200$ MeV.
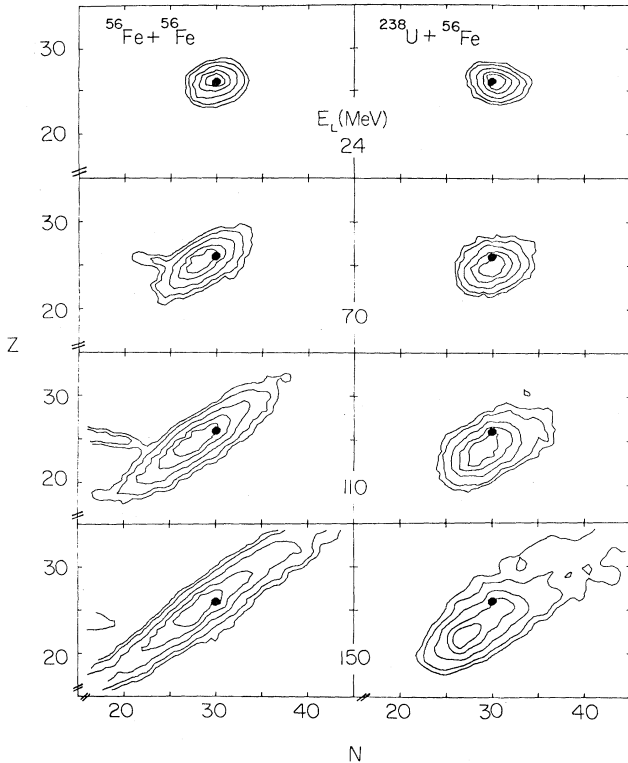
FIG. 2. Contour lines of measured cross section in the N-Z plane obtained in the ^{56}Fe + ^{56}Fe reaction at 8° and the ^{238}U + ^{56}Fe reaction at 45° for energy losses E_L of 24±2, 70±5, 110±5, and 150±5 MeV. The contour lines represent 75%, 50%, 25%, 10%, and 5% of the maximum cross section of each distribution. The filled circle indicates the location of the projectile $^{56}_{26}$Fe. The low-N tail near $Z = 26$ in the Fe + Fe reaction is due to elastically scattered projectiles which have been subsequently rescattered from the experimental structure.

tributions from sequential fission can be seen to produce the aforementioned tails.

Results of a two-dimensional Gaussian least-squares fit in the N-Z plane are given in Tables II to V and shown in Figs. 5 to 16. The fits were performed with the function

$$P(x',y') = h \exp\{ -\tfrac{1}{2}[a'(x'-\bar{x})^2 + b'(y'-\bar{y})^2]\} \ . \quad (1)$$

The variables x' and y' represent a coordinate system rotated by an angle ϕ with respect to the N-Z plane (compare Fig. 3) so that

$$x' = Z \cos\phi - N \sin\phi$$

and

$$y' = Z \sin\phi + N \cos\phi \ .$$

The slope $k = tg\phi$ defines the orientation of the y' axis and thus all major axes of the elliptical contour lines in Fig. 2 with respect to the N-Z plane. Note that in the x'-y' system the covariance vanishes: $\sigma_{x'y'} = 0$. For each E_L of a specific reaction, six parameters are obtained: a normalization h; the centroids of the proton and neutron distri-

butions, $\bar{x}$ and $\bar{y}$; two parameters a' and b', related to the variances of the distribution with respect to x' and y'; and the slope k. Fits were performed with limits of $P/h = 0.1$ except at the lowest E_L ($P/h = 0.02$, 0.04, 0.06, and 0.08 at $E_L = 8$, 12, 16, and 20 MeV, respectively). Uncertainties on all fit parameters were derived from the X^2-fit procedure. Further details may be found in Ref. 16.

It is important to correct the fit results a', b' and k for the experimental resolution of mass and charge identification and for the effects of binning which can in itself be strongly dependent on the experimental resolution. This is discussed in detail in Ref. 16. The values given in Tables II to V are corrected for these effects and all uncertainties on a', b', k, $\bar{N}$, and $\bar{Z}$ include the uncertainties in the experimental resolution as well as in the absolute calibration of mass and charge.

Data taken at different angles for the same projectile-target combination (Bi and U targets) were averaged since no significant differences in the results were observed. The normalization h, related to the angle-dependent cross section, has been omitted in Tables II to V. The tables show the results obtained for N-Z data. Some of the figures also show results for fits obtained from N'-Z data (corrected for neutron emission).

Quantities of interest both in the N-Z and A-Z plane can be calculated from the parameters given in Tables II to V. The equations necessary to obtain a variety of variances, covariances, and correlation coefficients and their uncertainties can be found in Ref. 16. For convenience, the definitions and equations of the quantities used in this paper will be given in the next section.

G. Definitions of variance-related quantities used in this paper

The quantities related to variances that are discussed in this paper are defined[16] in terms of the two-dimensional Gaussian function $P(a',b',k,\bar{N},\bar{Z})$ [see Eq. (1)], where all integrations have to be performed from $-\infty$ to $+\infty$. These include:

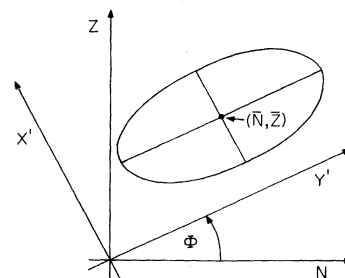(1) the total charge and neutron variances σ_Z^2 and σ_N^2,

FIG. 3. Diagram relating the x'-y' coordinate system used in Eq. (1) to the N-Z plane. The variables x' and y' are parallel to the minor and major axes with lengths $2/\sqrt{a'}$ and $2/\sqrt{b'}$, respectively, of the contour line with $P/h = e^{-1/2}$ of the two-dimensional Gaussian function P centered at $(\bar{N}, \bar{Z})$.

TABLE II. Parameters obtained with a two-dimensional Gaussian χ^2 fit [Eq. (1) in Sec. II F] to measured projectilelike fragment neutron-proton distributions originating from the ^{56}Fe + ^{56}Fe reaction at a laboratory angle of 8° as a function of total kinetic energy loss E_L. All parameters are corrected for experimental resolution and the effects of computer binning.

E_L (MeV)	$\bar{Z}$	$\bar{N}$	a'	b'	k
12	25.91±0.11	30.30±0.16	1.903±0.146	0.8905±0.0701	−0.165±0.078
16	25.93±0.10	29.95±0.15	1.589±0.083	0.6464±0.0304	0.010±0.039
20	25.86±0.10	29.82±0.15	1.185±0.061	0.6123±0.0292	0.149±0.014
24	25.88±0.10	29.69±0.15	1.132±0.058	0.5462±0.0267	0.259±0.057
28	25.88±0.11	29.61±0.15	1.185±0.067	0.5200±0.0318	0.498±0.073
32	25.74±0.11	29.49±0.15	1.013±0.052	0.4192±0.0234	0.515±0.059
36	25.68±0.11	29.45±0.15	1.148±0.066	0.3957±0.0247	0.585±0.061
40	25.59±0.11	29.39±0.15	1.146±0.067	0.3278±0.0225	0.670±0.058
44	25.51±0.11	29.19±0.15	1.178±0.061	0.3341±0.0192	0.682±0.051
48	25.37±0.11	29.01±0.15	1.173±0.067	0.2779±0.0184	0.679±0.050
52	25.40±0.11	28.94±0.15	1.163±0.064	0.2506±0.0157	0.735±0.045
56	25.32±0.11	28.81±0.15	1.293±0.074	0.2637±0.0166	0.720±0.046
60	25.26±0.12	28.69±0.16	1.294±0.087	0.2358±0.0191	0.725±0.052
64	25.07±0.11	28.51±0.16	1.203±0.073	0.2260±0.0158	0.714±0.047
70	24.83±0.11	28.20±0.16	1.205±0.065	0.1649±0.0100	0.735±0.032
80	24.60±0.12	27.97±0.16	1.237±0.066	0.1203±0.0072	0.749±0.025
90	24.31±0.12	27.58±0.16	1.289±0.065	0.0955±0.0054	0.761±0.020
100	24.12±0.12	27.30±0.17	1.311±0.066	0.0722±0.0042	0.780±0.018
110	23.93±0.13	27.18±0.17	1.383±0.070	0.0543±0.0030	0.785±0.014
120	23.78±0.12	26.98±0.17	1.286±0.058	0.0422±0.0020	0.791±0.011
130	23.73±0.13	26.91±0.18	1.337±0.063	0.0333±0.0016	0.809±0.010
140	23.54±0.15	26.69±0.19	1.224±0.056	0.0232±0.0012	0.807±0.009

$$\sigma_Z^2 = \frac{1}{n} \int (Z - \bar{Z})^2 P \, dN \, dZ = \gamma b \ , \qquad (2a)$$

$$\sigma_N^2 = \frac{1}{n} \int (N - \bar{N})^2 P \, dN \, dZ = \gamma a; \qquad (2b)$$

(2) the correlation coefficient ρ_{NZ} in terms of the covariance σ_{NZ},

$$\rho_{NZ} = \sigma_{NZ} / (\sigma_N \sigma_Z) = c \, (ab)^{-1/2} \ , \qquad (3)$$

TABLE III. Same as Table II for the ^{165}Ho + ^{56}Fe reaction at 30°.

E_L (MeV)	$\bar{Z}$	$\bar{N}$	a'	b'	k
8	25.87±0.10	30.57±0.16	10.395±0.916	1.1591±0.0959	−0.078±0.034
12	25.69±0.11	30.49±0.16	3.029±0.251	0.8514±0.0729	−0.066±0.050
16	25.52±0.11	30.42±0.15	1.960±0.141	0.8215±0.0624	0.045±0.064
20	25.44±0.11	30.40±0.15	1.809±0.119	0.7633±0.0500	0.059±0.055
24	25.39±0.11	30.36±0.15	1.395±0.098	0.7027±0.0499	0.132±0.066
28	25.25±0.11	30.22±0.15	1.534±0.099	0.6854±0.0458	0.426±0.078
32	25.12±0.11	30.08±0.15	1.222±0.073	0.5392±0.0334	0.342±0.064
36	25.10±0.11	30.03±0.15	1.302±0.088	0.5057±0.0369	0.448±0.072
40	24.92±0.11	29.93±0.15	1.045±0.058	0.4571±0.0277	0.501±0.071
44	24.87±0.11	29.83±0.15	1.065±0.067	0.4605±0.0312	0.561±0.083
48	24.82±0.11	29.71±0.15	1.190±0.079	0.4069±0.0305	0.485±0.067
52	24.71±0.11	29.57±0.15	1.213±0.071	0.3565±0.0235	0.653±0.060
56	24.62±0.11	29.54±0.15	1.092±0.071	0.3305±0.0352	0.614±0.064
60	24.55±0.11	29.45±0.15	1.179±0.077	0.3288±0.0248	0.640±0.066
64	24.45±0.12	29.33±0.16	1.192±0.095	0.3007±0.0271	0.575±0.066
70	24.31±0.11	29.21±0.16	1.033±0.066	0.2721±0.0200	0.650±0.059
80	24.09±0.11	29.00±0.16	1.046±0.064	0.2288±0.0164	0.713±0.051
90	23.84±0.12	28.66±0.16	1.099±0.068	0.1881±0.0134	0.747±0.044
100	23.70±0.12	28.57±0.17	1.081±0.071	0.1530±0.0119	0.728±0.041
110	23.45±0.13	28.44±0.18	1.195±0.092	0.1397±0.0136	0.692±0.043
120	23.15±0.13	28.13±0.18	1.107±0.087	0.1155±0.0107	0.659±0.038
130	23.07±0.14	27.93±0.19	1.325±0.099	0.0859±0.0075	0.675±0.029

TABLE IV. Same as Table II for the ^{209}Bi + ^{56}Fe reaction averaged for data obtained at 34° and 38°.

E_L (MeV)	$\bar{Z}$	$\bar{N}$	a'	b'	k
8	25.85±0.10	30.66±0.15	8.392±0.648	1.1505±0.0737	−0.127±0.032
12	25.72±0.11	30.58±0.16	3.871±0.363	1.0016±0.0934	−0.054±0.058
16	25.54±0.11	30.58±0.15	2.666±0.194	0.8881±0.0612	−0.039±0.052
20	25.37±0.11	30.63±0.15	1.904±0.144	0.8381±0.0618	0.003±0.075
24	25.36±0.11	30.54±0.15	1.499±0.118	0.6857±0.0549	0.269±0.094
28	25.19±0.11	30.51±0.15	1.292±0.091	0.6369±0.0487	0.410±0.100
32	25.18±0.11	30.53±0.15	1.254±0.079	0.5195±0.0359	0.318±0.070
36	25.04±0.11	30.40±0.15	1.171±0.082	0.4985±0.0366	0.245±0.072
40	24.99±0.11	30.36±0.15	1.197±0.089	0.4853±0.0384	0.342±0.075
44	24.82±0.08	30.34±0.12	1.089±0.070	0.4067±0.0281	0.316±0.059
48	24.80±0.08	30.23±0.12	1.178±0.072	0.4023±0.0281	0.422±0.058
52	24.74±0.08	30.21±0.12	1.007±0.060	0.3562±0.0238	0.378±0.055
56	24.60±0.08	30.04±0.12	1.035±0.064	0.3682±0.0266	0.466±0.065
60	24.55±0.08	30.08±0.11	0.916±0.056	0.3515±0.0239	0.498±0.045
64	24.57±0.09	29.92±0.12	0.950±0.061	0.2889±0.0216	0.581±0.064
70	24.36±0.08	29.86±0.11	0.897±0.039	0.2858±0.0139	0.547±0.042
80	24.19±0.08	29.69±0.11	0.965±0.045	0.2200±0.0114	0.552±0.033
90	23.96±0.08	29.52±0.12	0.901±0.043	0.1898±0.0103	0.590±0.033
100	23.70±0.08	29.22±0.12	0.939±0.044	0.1728±0.0094	0.624±0.031
110	23.60±0.09	29.17±0.12	1.159±0.060	0.1357±0.0085	0.666±0.029
120	23.34±0.09	28.91±0.13	1.023±0.056	0.1134±0.0073	0.698±0.029
130	23.21±0.10	28.78±0.13	0.948±0.054	0.0953±0.0064	0.704±0.028
140	22.94±0.10	28.44±0.14	0.990±0.059	0.0864±0.0062	0.701±0.027

TABLE V. Same as Table II for the ^{238}U + ^{56}Fe reaction averaged for data obtained at 40° and 45°.

E_L (MeV)	$\bar{Z}$	$\bar{N}$	a'	b'	k
8	25.83±0.07	30.54±0.10	5.693±0.299	1.2170±0.0502	−0.322±0.032
12	25.73±0.07	30.52±0.11	3.310±0.172	0.9380±0.0421	−0.285±0.036
16	25.69±0.07	30.53±0.10	2.518±0.111	0.9073±0.0351	−0.164±0.036
20	25.59±0.07	30.58±0.10	2.129±0.096	0.8507±0.0335	−0.098±0.040
24	25.47±0.07	30.59±0.10	1.785±0.078	0.8135±0.0330	−0.052±0.045
28	25.32±0.07	30.56±0.10	1.353±0.054	0.7597±0.0269	0.078±0.053
32	25.19±0.07	30.49±0.10	1.250±0.046	0.6861±0.0231	0.212±0.023
36	25.07±0.07	30.42±0.10	1.207±0.043	0.6152±0.0195	0.313±0.052
40	24.96±0.07	30.40±0.10	1.149±0.042	0.5636±0.0191	0.271±0.047
44	24.87±0.07	30.36±0.10	1.023±0.035	0.5220±0.0174	0.318±0.047
48	24.79±0.07	30.33±0.10	1.034±0.039	0.4516±0.0168	0.375±0.042
52	24.70±0.07	30.26±0.10	0.997±0.037	0.4344±0.0154	0.321±0.040
56	24.56±0.07	30.18±0.10	1.060±0.041	0.4254±0.0161	0.391±0.040
60	24.52±0.08	30.20±0.11	0.892±0.036	0.3726±0.0153	0.422±0.045
64	24.41±0.08	30.11±0.11	0.949±0.036	0.3654±0.0137	0.451±0.040
70	24.26±0.10	29.99±0.15	0.847±0.039	0.3048±0.0125	0.545±0.044
80	24.06±0.11	29.87±0.15	0.857±0.042	0.2771±0.0130	0.568±0.045
90	23.90±0.11	29.63±0.15	0.750±0.038	0.2263±0.0116	0.594±0.047
100	23.58±0.11	25.54±0.15	0.771±0.041	0.1891±0.0104	0.700±0.045
110	23.48±0.12	29.31±0.16	0.740±0.042	0.1506±0.0091	0.690±0.043
120	23.06±0.12	29.14±0.16	0.791±0.044	0.1306±0.0078	0.684±0.037
130	22.99±0.12	28.95±0.16	0.837±0.048	0.1102±0.0066	0.714±0.032
140	22.73±0.13	28.78±0.17	0.731±0.045	0.0864±0.0060	0.694±0.032
150	22.44±0.14	28.44±0.19	0.747±0.054	0.0783±0.0067	0.696±0.038
160	22.41±0.14	28.58±0.19	0.742±0.049	0.0575±0.0044	0.689±0.028
170	22.17±0.14	28.21±0.17	0.732±0.052	0.0540±0.0046	0.725±0.022
180	22.09±0.16	28.42±0.24	0.808±0.063	0.0409±0.0038	0.632±0.025

$$\sigma_{NZ} = \frac{1}{n} \int (N - \bar{N})(Z - \bar{Z}) P \, dN \, dZ = \gamma c \, , \quad (4)$$

$$n = \int P \, dN \, dZ,$$

$$\gamma = (ab - c^2)^{-1} \, ;$$

and

(3) the variances at constant N, Z, or A with x and y representing any combination of A, N, and Z,

$$\sigma_x^2(y) = \frac{1}{n_x} \int (x - \bar{x})^2 P \, dx, \quad n_x = \int P \, dx \, . \quad (5a)$$

More specifically,

$$\sigma_Z^2(N) = \sigma_A^2(N) = a^{-1} \, , \quad (5b)$$

$$\sigma_N^2(Z) = \sigma_A^2(Z) = b^{-1} \, , \quad (5c)$$

$$\sigma_Z^2(A) = \sigma_N^2(A) = (a + b + 2c)^{-1} \, . \quad (5d)$$

Note that $\sigma_x^2(y)$ is independent of y for a two-dimensional Gaussian function. The parameters a, b, and c can be calculated from a', b', and k:

$$a = (k^2 b' + a')/(k^2 + 1) \, , \quad (6a)$$

$$b = (k^2 a' + b')/(k^2 + 1) \, , \quad (6b)$$

$$c = k(a' - b')/(k^2 + 1) \, . \quad (6c)$$

Note that a, b, and c are the parameters that one would obtain with a fit of the function

$$P(N,Z) = h \exp - \tfrac{1}{2} [a(Z - \bar{Z})^2 + b(N - \bar{N})^2$$

$$+ 2c(Z - \bar{Z})(N - \bar{N})] \, , \quad (7)$$

i.e., a function defined in the N-Z plane.

III. RESULTS

Until recently only one-dimensional charge *or* mass spectra for damped heavy-ion reactions at fixed energy loss E_L could be determined experimentally. The centroids and variances extracted for these distributions as a function of E_L represent an important basis for the comparison between experimental data and theoretical calculations. The more recent data with simultaneous mass and charge determination have usually also been treated as one-dimensional data by performing cuts in the three-dimensional E_L, Z, and A space and determining centroids and variances of the resulting one-dimensional spectra. The charge centroids for fixed mass A, $\bar{Z}(A)$, for the ^{56}Fe + ^{56}Fe and the ^{238}U + ^{56}Fe reactions, shown in Fig. 4 as a function of E_L, give an example of results obtained from Gaussian fits to such one-dimensional spectra. This small sample of possible one-dimensional fit results demonstrates that such a procedure results in a large amount of secondary (fit) data. For a meaningful presentation and an easier interpretation it is desirable to compress the amount of these secondary data. This can be done by averaging the results over regions of one of the independent (gating) parameters where the fit values do not change significantly. Such a procedure has been chosen for a presentation of the data[1] for isobaric charge vari-

ances $\sigma_Z^2(A)$.

The observations[1,16] obtained from one-dimensional fits at a specific E_L that (a) $\sigma_Z^2(A)$ is nearly constant for the masses representing the major part of the cross section, and (b) $\bar{Z}(A)$ is a linear function of A, make it possible to perform the two-dimensional Gaussian fits outlined in Sec. II F. These two-dimensional fits also give an average description of the experimental data by using only a few uniquely defined parameters. Theoretical calculations can be compared either directly with these parameters or with quantities derived from them. In this paper, most of the results are obtained from these two-dimensional Gaussian fits and are presented as a function of E_L. In *all* cases the E_L scale includes the calculated corrections for neutron emission (Sec. II C and Ref. 16). In Figs. 5—16 results obtained from two-dimensional fits are represented by circles and triangles.

A. Centroids of the charge and neutron number distributions

The circles in Figs. 5 and 6 show the measured centroids of the charge, $\bar{Z}$, and neutron number, $\bar{N}$, distributions, respectively, as a function of E_L for all systems under investigation. These values, along with their uncertainties, can also be found in Tables II to V. Owing to the
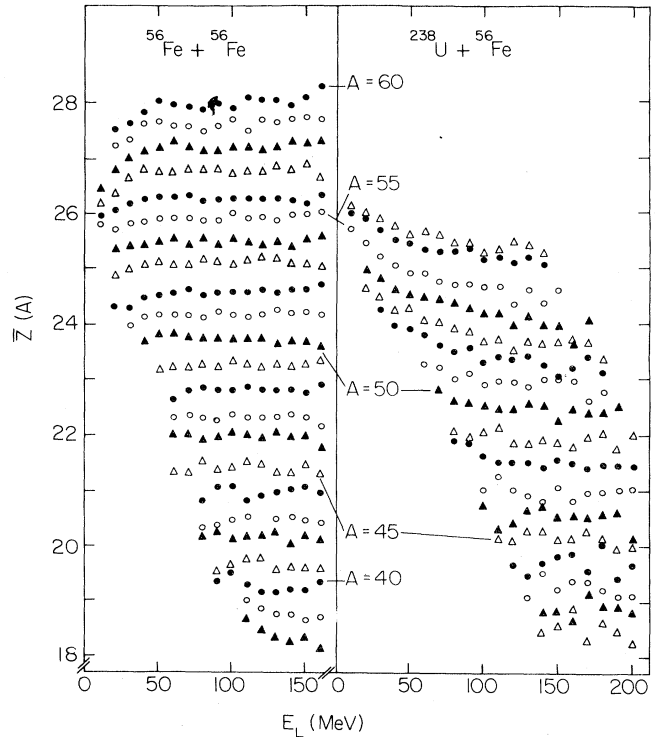

FIG. 4. Charge centroids for each mass, $\bar{Z}(A)$, obtained from Gaussian fits to one-dimensional charge distributions as a function of E_L for damped products detected in the ^{56}Fe + ^{56}Fe reaction at 8° and the ^{238}U + ^{56}Fe reaction at 45°. The charge distributions were created by accepting only products identified within ±0.3 units of a specific mass. Alternating symbols distinguish between different masses.
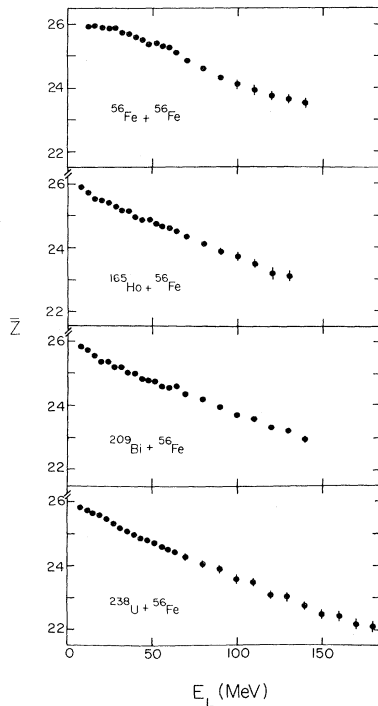
FIG. 5. Charge centroids as obtained from a two-dimensional Gaussian fit as a function of E_L for damped products obtained in the reactions indicated in the figure.
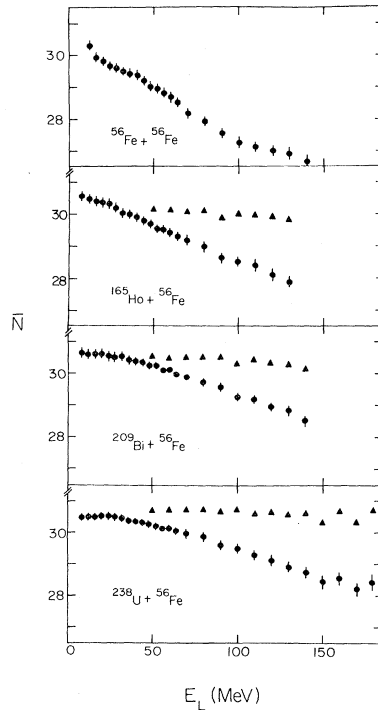
different processes responsible for the changes in $\bar{Z}$ and $\bar{N}$ with E_L, the results of the ^{56}Fe + ^{56}Fe reaction will be discussed separately from those obtained for the asymmetric systems.

1. Centroids of the charge and neutron number distributions for the $^{56}Fe + ^{56}Fe$ reaction

The primary damped reaction products obtained from the symmetric reaction ^{56}Fe + ^{56}Fe are expected to yield charge and neutron number distributions which are symmetric about $Z = 26$ and $N = 30$ if preequilibrium decay can be excluded. Any deviation of $\bar{Z}$ and $\bar{N}$ from these values can then be attributed to secondary particle emission.[16] It can be seen in Figs. 5 and 6 that both $\bar{Z}$ and $\bar{N}$ decrease with increasing E_L due to emission of neutrons and charged particles. $\bar{N}$ already begins to decrease at smaller E_L than does $\bar{Z}$, indicating that the neutron decay channel opens at smaller excitation energies than does the proton (and α) channel. This can be expected from the neutron-to-proton ratio of this system of $N/Z = 1.15$. Owing to dominant neutron emission at low E_L the average fragment $\bar{N}/\bar{Z}$ ratio decreases with E_L (Fig. 7) until an equilibrium between proton and neutron decay is achieved at approximately $N/Z = 1.13$ for $E_L \gtrsim 50$ MeV. To preserve $\bar{N}/\bar{Z}$ at higher E_L it is necessary to emit

FIG. 6. Same as Fig. 5 for the centroids of the neutron number of the projectilelike fragments. Filled circles represent the measured data. Triangles indicate the calculated neutron centroids of the fragments before deexcitation by neutron evaporation.
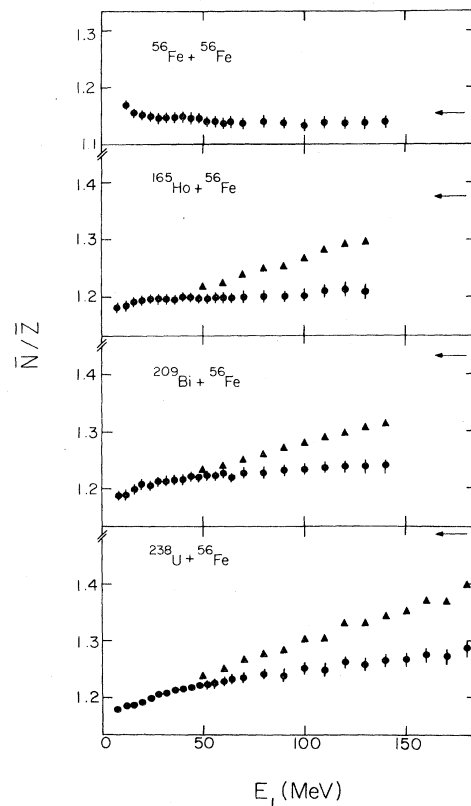

FIG. 7. Ratios of the data shown in Figs. 5 and 6. The arrows indicate the N/Z ratio of the compound nucleus for the respective reactions.

about 13% more neutrons than protons, which results in the larger slope for $\bar{N}$ as a function of E_L than observed for $\bar{Z}$ in Figs. 5 and 6.

2. Centroids of the charge and neutron number distributions for the asymmetric reactions

For the asymmetric reactions ^{165}Ho, ^{209}Bi, and ^{238}U + ^{56}Fe the primary reaction mechanisms can modify $\bar{Z}$ and $\bar{N}$ in addition to secondary particle emission. Fortunately, for these systems charged-particle decay is strongly suppressed[16,34] relative to neutron emission. Thus, an estimate of the primary average fragment neutron number $\bar{N}'$ can be made (Sec. II C, Ref. 16), while the measured $\bar{Z}$ should be nearly identical to the primary average fragment charge.

For all asymmetric systems $\bar{Z}$ decreases linearly with E_L (Fig. 5). The rate of decrease is nearly the same for the Ho, Bi, and U targets, i.e., 2.25 ± 0.10 Z units per 100 MeV of E_L. This indicates that protons are preferentially transferred from projectile to target independently of target mass or neutron excess in the target. In Fig. 6 the average neutron number $\bar{N}$ is observed to decrease with E_L similar to $\bar{Z}$, however, with rates depending on the target. After correction for neutron evaporation, $\bar{N}'$ exhibits a completely different behavior than $\bar{Z}$; $\bar{N}'$ is nearly constant with E_L for all heavy targets. There seems to be a slight decrease in $\bar{N}'$ for the Ho and Bi targets; no change can be observed for the U target. A second feature is important: Within the first 10 MeV of E_L there is an immediate increase of $\bar{N}$ of about 0.5 units for all systems. For these low energy losses the ground state Q values[43] Q_{gg} allow only for neutron pickup if Z remains unchanged. Hence, the data indicate that neutron pickup is an important reaction process during the initial stages of the interaction.

The measured data, especially for the Bi and U targets, exhibit constant $\bar{N}$ values up to about 25 MeV of E_L and then $\bar{N}$ starts to decrease. This can be taken as evidence that neutron emission becomes possible at about 25 to 30 MeV of E_L corresponding to slightly more than 6 MeV of excitation energy in the projectilelike fragment if the excitation energy divides according to mass.

3. Average neutron-to-proton ratios for the asymmetric reactions

The relative behavior of the average neutron and proton numbers, the $\bar{N}/\bar{Z}$ ratios, is shown in Fig. 7. For the asymmetric reactions both $\bar{N}/\bar{Z}$ and $\bar{N}'/\bar{Z}$ increase with E_L, mainly due to the dominant decrease of $\bar{Z}$ with E_L. Above about 10 MeV a nearly linear dependence of the ratios on E_L is found, with $\bar{N}'/\bar{Z}$ increasing at rates 0.10 (Ho), 0.11 (Bi), and 0.12 (U target) per 100 MeV of E_L. This results in a dramatic increase of neutron excess at a rate of between 2.5 and 3.2 neutrons per 100 MeV of E_L for nuclear charges of about 26, and a significant decrease in the average neutron binding energy of projectilelike fragments with E_L. However, in none of the asymmetric reactions does the $\bar{N}'/\bar{Z}$ ratio come close to the N/Z ratio

of the combined system indicated by arrows in Fig. 7.

The initial increase in $\bar{N}$ is also reflected in a rapid increase of $\bar{N}/\bar{Z}$ from that of the projectile (1.15) to ≥ 1.20 within the first 20 MeV of E_L. In the Ho + Fe reaction neutron emission above about 25 MeV E_L just compensates a further increase in $\bar{N}'/\bar{Z}$. For Fe + U, the number of neutrons emitted cannot compensate completely for the original increase in neutron excess, so that even $\bar{N}/\bar{Z}$ increases with E_L. This makes, for example, the Fe + U reaction an excellent means of producing neutron-rich isotopes which have a high probability of surviving the deexcitation process.[17]

4. Charge centroids as a function of mass

The centroids $\bar{Z}(A)$ obtained from one-dimensional fits (Fig. 4) may be compared with the $\bar{N}/\bar{Z}$ values of Fig. 7. While Fig. 7 gives a measure for the neutron excess averaged over all fragments, Fig. 4 allows one to observe this property for individual fragment masses. A decrease of $\bar{Z}(A)$ in Fig. 4 corresponds to an increase of $\bar{N}/\bar{Z}$ in Fig. 7. Figure 4 shows that the change in neutron excess and thus the evolution of charge equilibration with E_L is qualitatively the same for all masses and is also in qualitative agreement with the average $\bar{N}/\bar{Z}$ values in Fig. 7. Specifically, $\bar{Z}(A)$ for all A have approximately constant values above about 50 MeV of E_L for the ^{56}Fe + ^{56}Fe reaction; for the ^{238}U + ^{56}Fe reaction the $\bar{Z}(A)$ values for all masses decrease with E_L within the experimental uncertainties which can be estimated from the fluctuations of the data points. The neglect of corrections for neutron emission in the data of Fig. 4 does not modify these conclusions.

Quantitative information about the degree of neutron excess in projectilelike fragments as a function of fragment mass can be found in Fig. 8 where the mass is divided by the respective $\bar{Z}(A)$ and averaged for $50 \leq E_L \leq 150$ MeV. The resulting

$$A/\bar{Z}(A) = N/\bar{Z}(A) + 1.0$$

values increase slowly and monotonically with A for fragments from the ^{56}Fe + ^{56}Fe reaction. Thus, the equilibri-
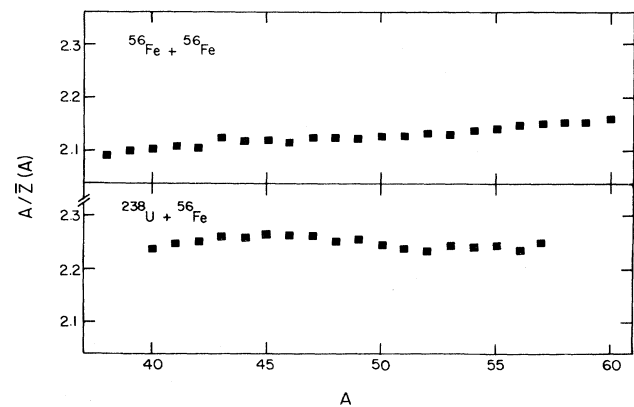

FIG. 8. The average mass to charge ratio $A/\bar{Z}(A)$ averaged over the range $50 \leq E_L \leq 150$ MeV as a function of fragment mass A. The uncertainties are smaller than the size of the data points.

um value of N/Z between proton and neutron evaporation possibly increases slowly with A. On the other hand, in this representation $A/\bar{Z}(A)$ may also exhibit properties of the reaction mechanism. The symmetric entrance channel only requires that this ratio for the primary reaction products be symmetric with respect to $A=56$ and $Z=26$. Thus, low ratios for $A<56$ may correspond to high ones for $A>56$. The ground state Q_{gg} values which dominate the potential energy surface make such a dependence of $A/\bar{Z}(A)$ on A for the primary reaction process probable.

For the ^{238}U + ^{56}Fe reaction $A/\bar{Z}(A)$ does not depend as strongly on A (lower part of Fig. 8). The small oscillations in $A/\bar{Z}(A)$ for this reaction are artifacts of the averaging procedure: Since $\bar{Z}(A)$ is not constant as a function of E_L (Fig. 4), averaging produces a bias related to the changing reaction cross sections for individual masses at different E_L. Nevertheless, the high average $A/\bar{Z}(A)$ ratio of >2.2 is apparent for *all* masses in the lower part of Fig. 8. Also, the charge equilibrium process seems to proceed nearly independently of A, as seen by the negligible dependence of $A/\bar{Z}(A)$ on A. The inclusion of corrections for neutron emission would modify the absolute values of $A/\bar{Z}(A)$, but leave its dependence on A nearly unaffected [i.e., $A/\bar{Z}(A)$ would be decreased for high A more strongly than for low A].

5. The slope of the N-Z distributions

Figure 7 shows the detailed dependence of the $\bar{N}/\bar{Z}$ ratio (and thus also the $\bar{A}/\bar{Z}$ ratio) on E_L averaged over all fragment masses, while Fig. 8 presents the dependence on A averaged over a wide range of E_L. Intimately related to both Figs. 7 and 8 is Fig. 9, which shows the alignment of two-dimensional fragment distributions in the N-Z plane as a function of E_L, expressed as the slope k of the major axis of the distribution in this plane [compare the discussion of Eq. (1)]. With this definition of k one finds that

$$N/\bar{Z}(N)=N/(\bar{Z}-k\bar{N}+kN) . \qquad (8)$$

Only for the special case that

$$k=\bar{Z}/\bar{N}=[N/\bar{Z}(N)]^{-1}$$

are the average neutron-to-proton ratios $N/\bar{Z}(N)$ [and also $A/\bar{Z}(A)$] independent of N and A. This condition is equivalent to the requirement that the major axis of the distribution goes through the origin of the N-Z plane. The approximation $k=\bar{Z}/\bar{N}$ can be helpful to obtain mass variances from charge variances with certain assumptions about the degree of correlation between proton and neutron exchange.[9] However, Fig. 9 shows that both k and k' are always smaller than the respective $(\bar{N}/\bar{Z})^{-1}$ and $(\bar{N}'/\bar{Z})^{-1}$ values which can be extracted from Fig. 7 or Tables II to V. Thus, this condition is never completely fulfilled for the present data. For low E_L, where k is rapidly changing, it is obvious that the assumption of $k=\bar{Z}/\bar{N}$ is not appropriate.

For all reactions shown in Fig. 9 the slopes k (for measured N-Z distributions) and k' (for calculated primary data) show a rapid increase at low E_L values and approach nearly constant values at high E_L. Note especially that the slopes change sign between about 15 and 30 MeV of
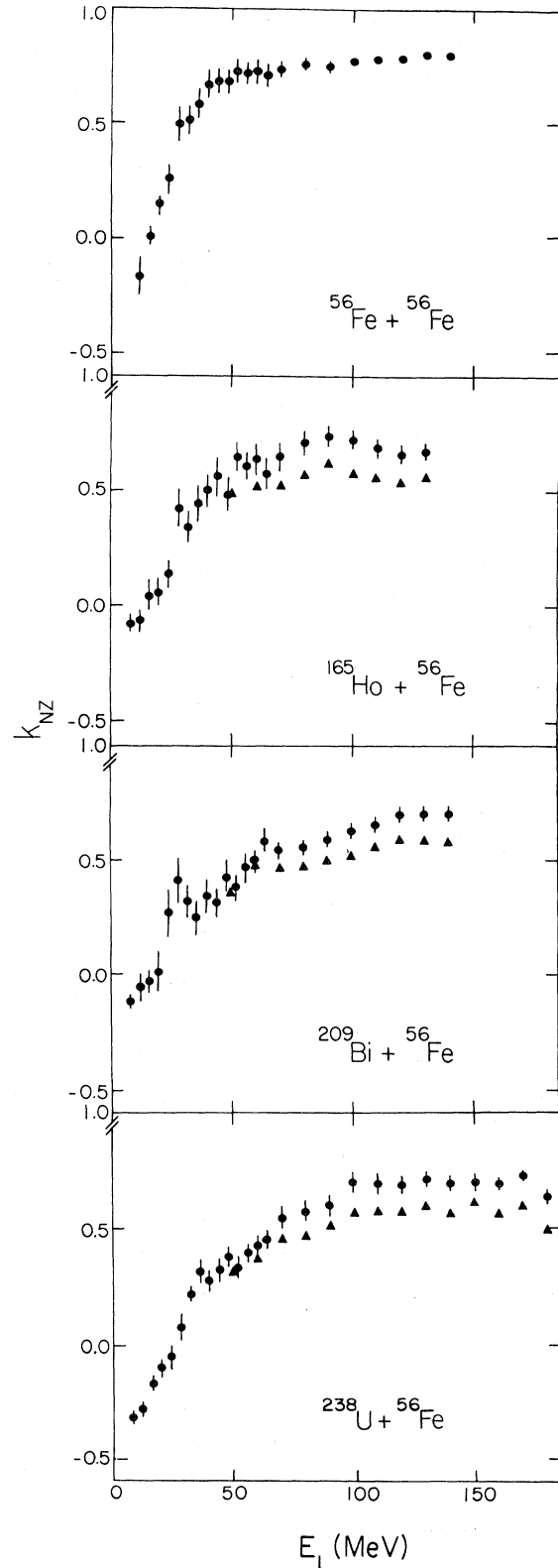

FIG. 9. The slope k_{NZ} of the major axis of the neutron-proton distributions as a function of E_L for projectilelike fragments obtained from the reactions indicated in the figure.

E_L for all systems, indicating a change from anticorrelated to correlated nucleon exchange (see Sec. III B 2). The transition from rapid change to nearly constant k occurs at E_L values which depend on the target, i.e., from about 40 MeV for the Fe target, to ~ 50 MeV for Ho, to above ~ 70 for Bi, and about 100 MeV for the U target. For Fe + Fe, k seems to continue to increase slightly with E_L within the nearly constant region. Of course, the influence of particle emission is not fully known here. The Fe + U reaction, however, exhibits a constant slope both prior to and after evaporation (k' and k) above 100 MeV of E_L. The absolute values of k and k' at high E_L are remarkably similar for all asymmetric systems; $k = 0.70$ and $k' = 0.58$. For the Fe + Fe system, however, k is larger at high E_L than for the asymmetric reactions and increases from about 0.74 to 0.80.

B. Variances of the fragment distributions

The three variables $\bar{N}$, $\bar{Z}$, and k are sufficient to obtain any centroid of the fragment mass, charge, or neutron number distribution at a specific energy loss E_L. Only two more variables (and an additional normalization) are needed to specify the distribution completely in the two-dimensional Gaussian representation. The additional parameters a' and b' [Tables II to V, Eq. (1)] which represent the inverse of the variances parallel and perpendicular to the axis defined by k can be such additional parameters. With a', b', and k any variance of interest of the system can be calculated [Eqs. (2)–(5) and Ref. 16]. Since the variances of the distribution are completely determined by three parameters (a',b',k), *no additional* information is obtained by the determination or calculation of additional variances, although it may prove to be much easier to interpret variances different from the one defined by a' and b'.

In this section several quantities related to the variances of the charge and neutron number distributions are presented. Some other quantities that can be calculated[16] have been presented previously.[9]

1. The total variances of the fragment distributions

The most commonly measured variances, the charge variances σ_Z^2, integrated over all masses ("total" variances), are shown as a function of E_L in Fig. 10. The total charge variances obtained from two-dimensional fits may be somewhat smaller than the ones obtained from one-dimensional fits,[35] since in two dimensions fission events can be excluded nearly quantitatively whereas in one dimension this is often not possible.

The total variances σ_Z^2 exhibit a dependence on E_L that is well known from many reactions to be a continuously increasing function of E_L, starting with σ_Z^2 consistent with zero at $E_L = 0$ and evolving to very wide charge distributions near the Coulomb barrier of the interacting nuclei (arrows in Fig. 10). For all asymmetric reactions the variances are very similar in absolute value at all E_L. For the ^{56}Fe + ^{56}Fe reaction, however, σ_Z^2 is nearly twice as large as for the asymmetric systems. This difference increases with E_L.

The total neutron variances σ_N^2, shown in Fig. 11, have a dependence on E_L similar to σ_Z^2. However, σ_N^2 exhibits a rapid initial increase of approximately one unit within the first 10 MeV of E_L in all reactions (assuming that σ_N^2 vanishes at $E_L = 0$). For the ^{56}Fe + ^{56}Fe reaction σ_N^2 is also larger at all E_L than for the asymmetric reactions, although for $E_L \lesssim 70$ MeV the differences in σ_N^2 are not as pronounced as in σ_Z^2.

The calculated primary neutron number variances of the asymmetric systems (triangles in Fig. 11) show that particle decay tends to narrow the distributions. This is due to the increase in the number of nucleons evaporated with increasing projectilelike fragment mass (carrying increasing excitation energy). Thus, if proton or alpha-particle decay is present[44] in addition to neutron decay
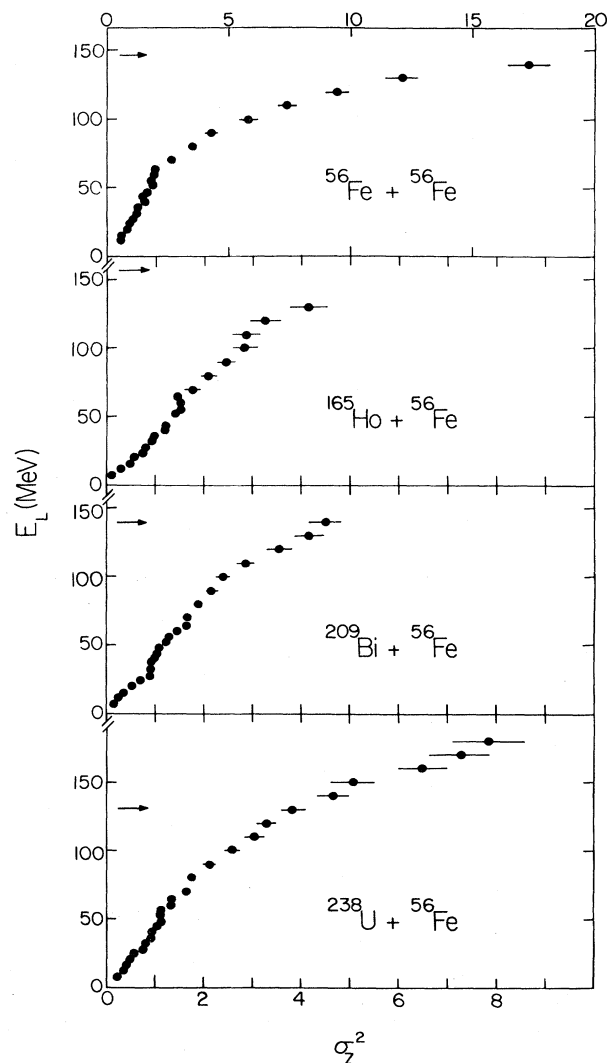
FIG. 10. Total charge variances as a function of E_L for the measured damped reaction products originating from the reactions indicated in the figure. Variances were obtained from two-dimensional Gaussian fits to the data. The arrows indicate the Coulomb barrier of spherical projectile-target nuclei at the distance of the combined strong interaction radii. Note that there is a change of scale for the ^{56}Fe + ^{56}Fe reaction.
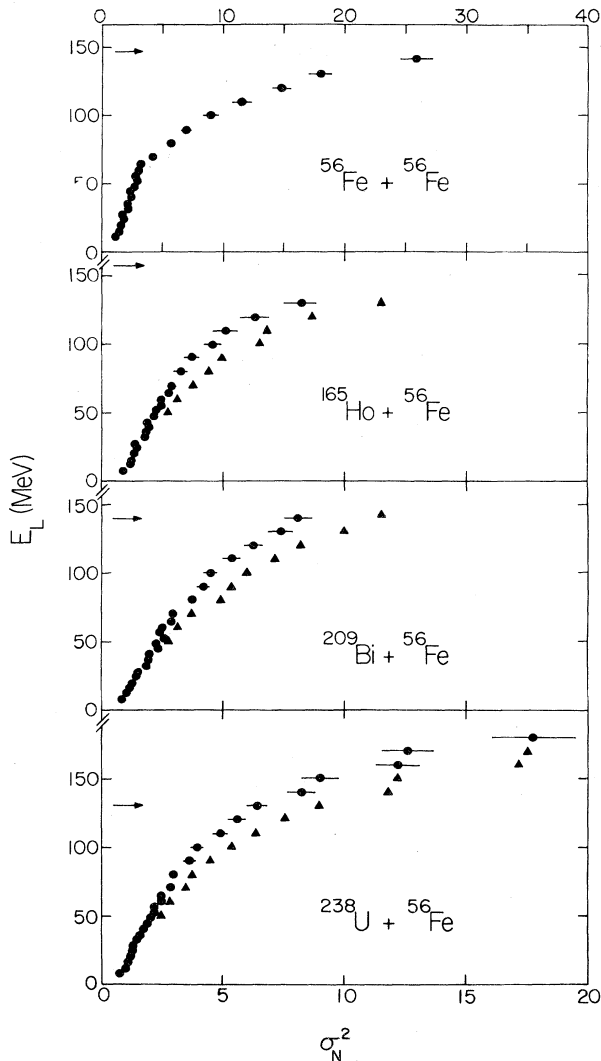
FIG. 11. Same as Fig. 10 for the variances of the total neutron number distributions. The triangles represent the calculated primary neutron variances. Note that there is again a change of scale for the ^{56}Fe + ^{56}Fe reaction.

FIG. 12. Ratios of the variances of the total neutron and proton number distributions shown in Figs. 10 and 11.

(^{56}Fe + ^{56}Fe reaction), the primary total charge distributions can also be expected to be wider than the measured ones.

A detailed comparison between the absolute values of charge and neutron number variances is demonstrated by the ratio σ_N^2/σ_Z^2, shown in Fig. 12. Above about 30 MeV of E_L this ratio for the detected fragments (circles) is nearly constant for all reactions with a value between 1.5 and 2.0. For the ^{56}Fe + ^{56}Fe reaction σ_N^2/σ_Z^2 seems to be somewhat lower (1.5) than for the asymmetric reactions. At high E_L the ratio of the variances appears to increase in the ^{165}Ho and ^{238}U + ^{56}Fe reactions. The triangles in Fig. 12 show that particle evaporation can influence these ratios significantly. Assuming pure neutron evaporation from projectilelike fragments in the asymmetric reactions indicates that σ_N^2/σ_Z^2 for high E_L is between 2.0 and 2.5.

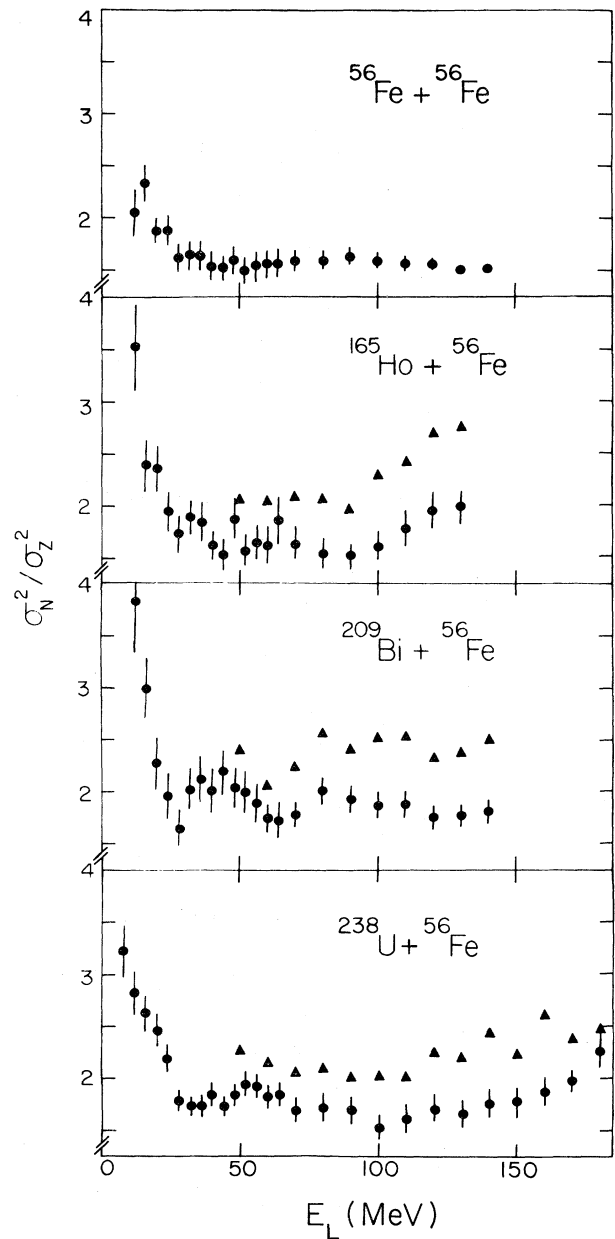The most prominent feature in Fig. 12 is the very high ratio σ_N^2/σ_Z^2 at low E_L. This can be expected from the initial rapid increase of σ_N^2 (Fig. 11) below $E_L = 10$ MeV, which is not present for σ_Z^2 (Fig. 10). The enhanced σ_N^2/σ_Z^2 ratios are clearly visible for all asymmetric reactions in Fig. 12 below about 20 MeV of E_L. For the ^{56}Fe + ^{56}Fe reaction the data may indicate the same feature although the lowest E_L data point does not follow the trend of increasing ratio with decreasing E_L.

The σ_A^2/σ_Z^2 ratios show very little or no enhancement at low E_L,[9,16] completely different from the σ_N^2/σ_Z^2 behavior. Also, no rapid increase of σ_A^2 at low E_L is observable.[9] This emphasizes the need for *simultaneous* mass and charge determination of each fragment if one is interested

in the properties of the neutron number distributions of reaction fragments.

2. The correlation coefficient

Figure 2 shows that the proton and neutron numbers of the reaction fragments are not independent of each other; they are confined to a limited area near a diagonal in the N-Z plane. The degree of correlation in proton and neutron number for all detected projectilelike fragments can be quantified by the correlation coefficient ρ_{NZ} [Eq. (3)] which may vary between -1 and $+1$. The correlation coefficients for all reactions under investigation here are shown in Fig. 13 as a function of E_L. A comparison of the distributions for ρ_{NZ} (Fig. 13) and the slope k (Fig. 9) shows a very similar appearance, since ρ_{NZ} is strongly dependent on k (e.g., $k=0$ leads necessarily to $\rho_{NZ}=0$). However, ρ_{NZ} contains in addition the properties of the distribution of the cross section around the axis defined by k.

For all reactions ρ_{NZ} approaches the limit of fully correlated neutron-proton distributions ($\rho_{NZ} \rightarrow +1$) at high E_L, where σ_Z^2 and σ_N^2 are the largest. For the ^{56}Fe + ^{56}Fe reaction ρ_{NZ} increases faster with E_L than for the asymmetric reactions due to the larger total variances at all E_L.

For low E_L Fig. 13 shows a smooth transition of ρ_{NZ} from anticorrelated ($\rho_{NZ} < 0$) to correlated ($\rho_{NZ} > 0$) proton-neutron distributions. The energy loss where ρ_{NZ} changes sign (identical to the one where k changes sign) increases systematically from about 16 MeV for ^{56}Fe + ^{56}Fe to about 24 MeV for the ^{238}U + ^{56}Fe reaction. From Fig. 2 one can deduce this transition from negative to positive correlation coefficients directly. For the ^{238}U + ^{56}Fe reaction at 24 MeV a negative slope of the major axis is apparent, whereas at high E_L the slope is positive. In the ^{56}Fe + ^{56}Fe reaction at 24 MeV of E_L the distribution is nearly circular and may be aligned with the N axis, indicating a correlation coefficient close to zero. The negative correlation coefficient may signify that in the early stages of the reaction protons and neutrons are preferentially transferred in opposite directions. A negative ρ_{NZ} may also be a consequence of the ground state Q values Q_{gg} of the reaction products. At low E_L even small differences in Q_{gg} may be of major importance for the transfer cross section. An attempt has been made to fit distributions obtained for constant total excitation energy E_t^* defined by $E_t^* = E_L - Q_{gg}$. This resulted in correlation coefficients which are consistent with $\rho_{NZ} = 0$ at $E_t^* = 0$ for the ^{238}U + ^{56}Fe reaction. This analysis is fragmentary, though, since only a limited number of the needed Q_{gg} values are available.[43]

The difference between ρ_{NZ} for detected fragments and for the estimated primary fragments is too small to be detectable in Fig. 13. However, if both neutron and charged-particle emission are present as expected for the ^{56}Fe + ^{56}Fe reaction, ρ_{NZ} of the primary reaction fragments may differ significantly from ρ_{NZ} of the detected fragments.[44] The mass-charge correlation coefficients ρ_{AZ} (open circles in Fig. 13) differ strongly from ρ_{NZ}. Most significantly, no negative ρ_{AZ} values are measured.
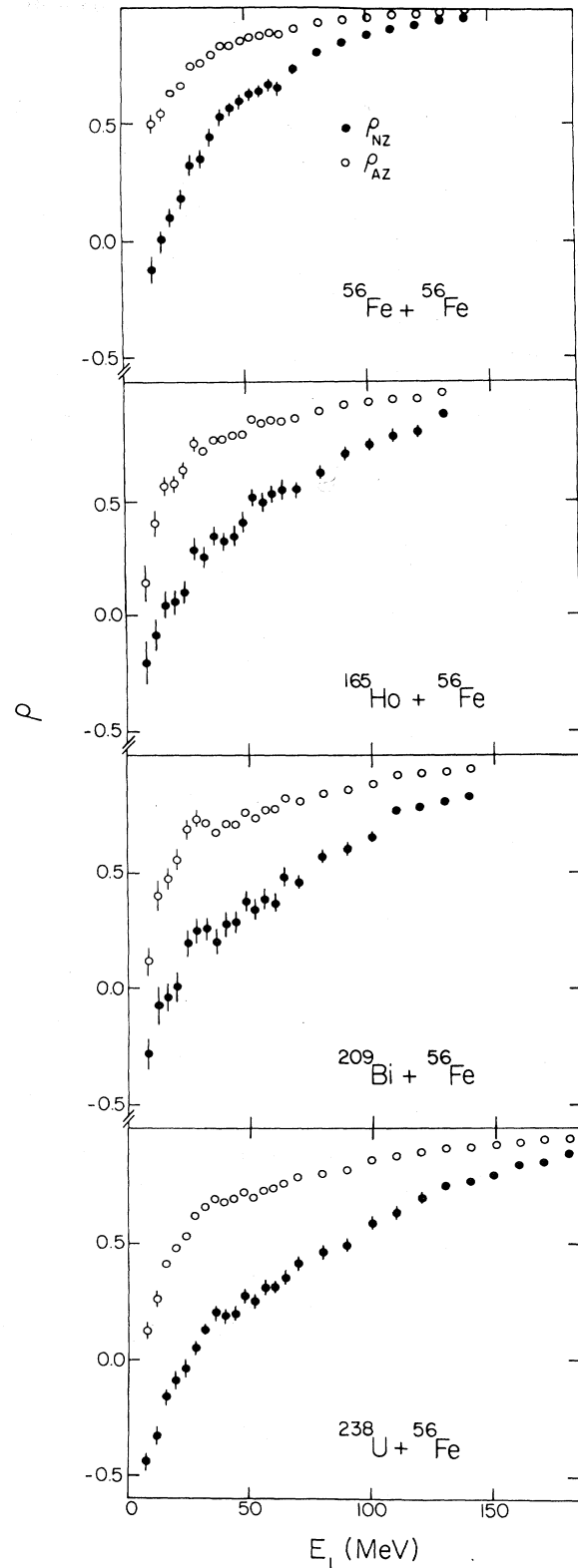

FIG. 13. The correlation coefficient ρ_{NZ} (solid circles) and ρ_{AZ} (open circles) as a function of E_L as obtained from a two-dimensional Gaussian fit to the neutron-proton distributions of damped products obtained in the reactions indicated in the figure.

3. Variances for fixed mass, charge,
and neutron number as a function of energy loss

Just as σ_Z^2, σ_N^2, and ρ_{NZ} constitute a complete set of parameters to define the distribution of cross sections around a centroid $(\overline{N}, \overline{Z})$ in the N-Z plane, so do the three variances which can be defined for constant neutron, proton, and mass number, $\sigma_Z^2(N)$, $\sigma_N^2(Z)$, and $\sigma_Z^2(A)$, defined by Eq. (5). These variances, obtained from a two-dimensional Gaussian fit, are equivalent to the weighted average of all corresponding variances at fixed N, Z, or A, respectively. Differences in absolute values in this work from those shown in Ref. 3 can be attributed mainly to differences in the fit function used and the range over which the data have been averaged.[16]

Inspection of Tables II to V shows that a', a measure of the width of the N-Z distribution perpendicular to its major axis, becomes nearly constant for high E_L. Thus, if the orientation of the major axis, (e.g., k) remains constant, one expects that any cut which is not parallel to the major axis will result in nearly constant variances for sufficiently large E_L.

Figures 14—16 show that all variances at constant N, Z, and A have a similar shape as a function of E_L: A rapid increase at low E_L followed by nearly constant variances at high E_L. The isotopic neutron variances $\sigma_N^2(Z)$ for the $^{238}U + ^{56}Fe$ reaction in Fig. 15 may still be increasing even at the highest E_L.

In general, one finds that the variances at high E_L are largest for $\sigma_N^2(Z)$ with values between 2 and 4 and small-
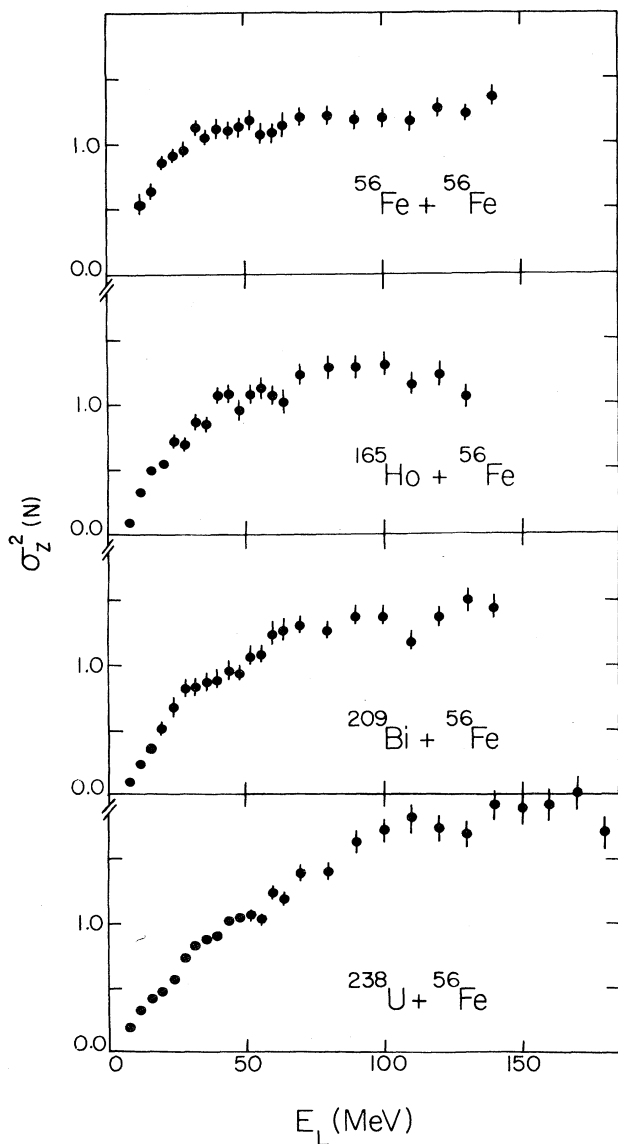

FIG. 14. Average isotonic variances $\sigma_Z^2(N) = \sigma_A^2(N)$ as a function of E_L of damped reaction products measured in the reactions indicated in the figure. These variances were obtained by two-dimensional Gaussian fits.
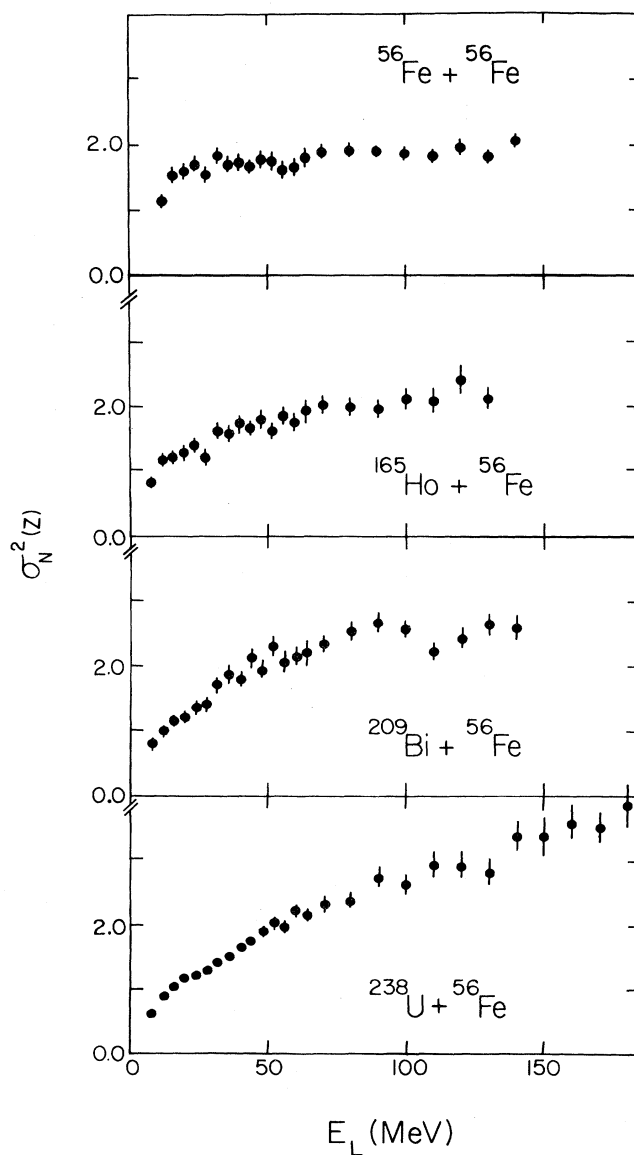

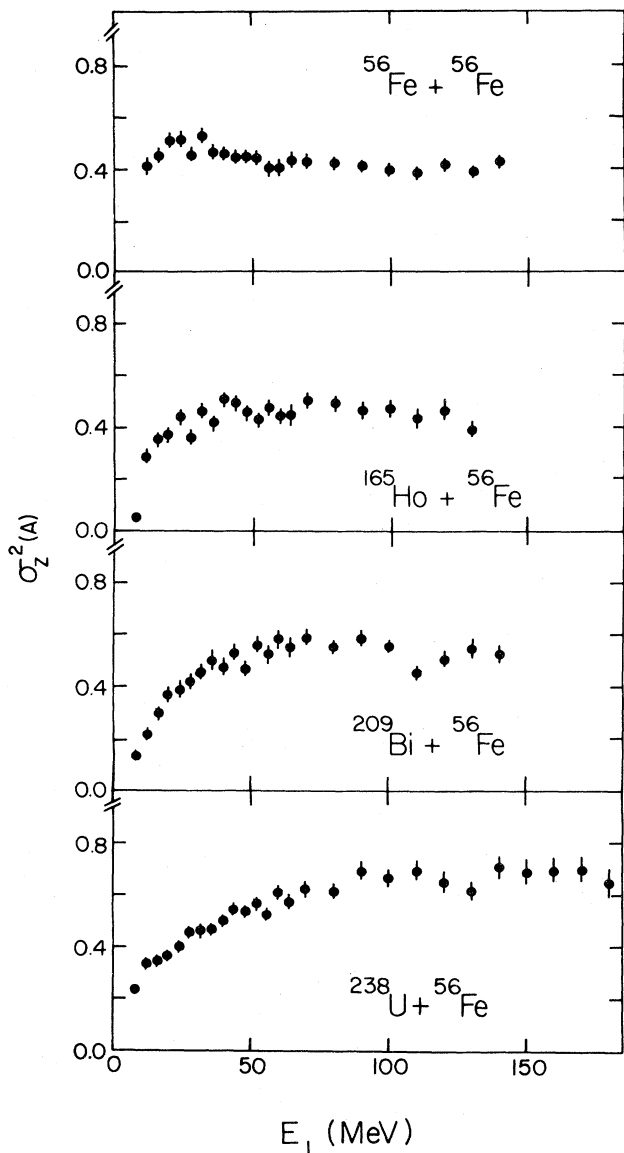FIG. 15. Same as Fig. 14 for the average isotopic variances $\sigma_N^2(Z) = \sigma_A^2(Z)$.

FIG. 16. Same as Fig. 14 for the average isobaric variances $\sigma_Z^2(A) = \sigma_N^2(A)$.

est for $\sigma_Z^2(A)$ ranging from 0.4 to 0.7. The intermediate isotonic charge variances $\sigma_Z^2(N)$ have values between about 1.2 and 2.0. The isobaric charge variances $\sigma_Z^2(A)$ approximate a projection onto the minor axis most closely for a wide range of E_L and are thus closest to $1/a'$.

A comparison of the different projectile-target combinations shows that (a) the rate of increase in variance at low E_L decreases with increasing target mass, and (b) the saturation variances at high E_L increase with target mass by about 70% from the ^{56}Fe to the ^{238}U target. For $\sigma_Z^2(A)$ of the ^{56}Fe + ^{56}Fe reaction (Fig. 15) there may even be a maximum in the variances at about 25 MeV of E_L.

For the variances in Figs. 14—16, no values are shown that include the estimates about particle evaporation. These *small* variances may be rather seriously influenced by the *details* of the particle decay processes,[12,44] e.g., the

binding energies of all individual (also intermediate) nuclei.

4. Isobaric charge variances as a function of fragment mass

Although the two-dimensional fit procedure yields a good average representation for the major part of the cross section of the N-Z fragment distributions, any fine structure in the data is lost. To investigate if such structure exists, the isobaric charge variances obtained from one-dimensional fits are displayed in Fig. 17 as a function of fragment mass for the ^{56}Fe + ^{56}Fe and ^{238}U + ^{56}Fe reactions. All variances in Fig. 17 are averaged over $60 \leq E_L \leq 180$ MeV.

The values for $\sigma_Z^2(A)$ between about $A = 50$ and 55 (the major part of the cross section is found in this range) are consistent with the variances shown in Fig. 16 at high E_L. However, the investigation of $\sigma_Z^2(A)$ over a very large range of A, far into the tails of the distributions, exhibits a systematic increase in $\sigma_Z^2(A)$ with mass at a rate of about 0.013 per mass unit. While $\sigma_Z^2(A)$ is consistent with a monotonic increase as a function of A for the ^{238}U + ^{56}Fe reaction, in the symmetric reaction ^{56}Fe + ^{56}Fe the magnitude of $\sigma_Z^2(A)$ alternates strongly with A. This alternation is not a consistent odd-even effect: At $45 < A < 55$ even masses show higher than average variances. On either side of this range the relation is inverted. There is no apparent correlation of the structure in $\sigma_Z^2(A)$ with nuclear shell structure.

For an explanation of the structure in Fig. 17 it may be important that nuclear charges do not form a continuous distribution but rather exist only in discrete units. Narrow distributions (upper part of Fig. 17) may be more strongly influenced by this effect than wider distributions are (lower part of Fig. 17). In fact, if one compares $\sigma_Z^2(A)$ for the ^{56}Fe + ^{56}Fe reaction with the position of its centroid with respect to the next integral Z number (Fig. 18), one finds that distributions with small variances are centered
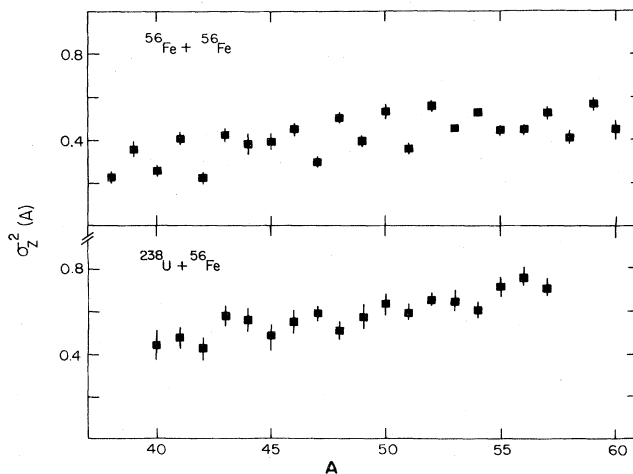

FIG. 17. Isobaric charge variances for individual masses obtained from one-dimensional Gaussian fits to charge distributions measured in the reactions indicated, averaged over the range $60 \leq E_L \leq 180$ MeV, are shown as a function of A.
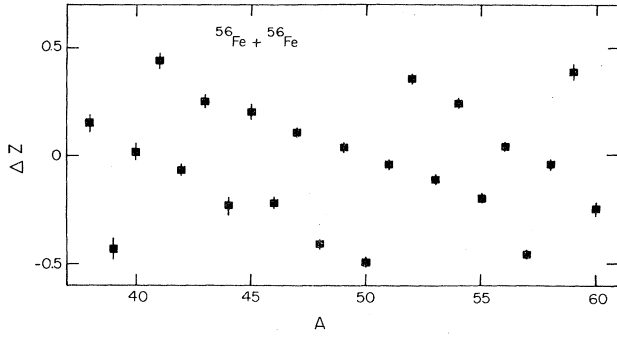
FIG. 18. The closest integer value has been subtracted from the measured charge centroids $\bar{Z}$ of the distributions, of which the variances are shown in Fig. 17, to yield ΔZ as a function of A [i.e., in FORTRAN notation: $\Delta Z = \bar{Z} - \text{INT}(\bar{Z} + 0.5)$].

near integral Z numbers ($\Delta Z \approx 0$), while the ones with large variances are centered between adjacent Z ($\Delta Z \approx \pm 0.5$). Since $2\bar{Z} < \bar{A}$, the relation between high $\sigma_Z^2(A)$ and odd or even A changes twice within the range of A in Fig. 17. Thus, the data are consistent with $\sigma_Z^2(A)$ which would increase monotonically with A for continuous Z distributions, which are, however, modulated depending on $\bar{Z}$ due to the discreteness of nuclear charges.

The structure in $\sigma_Z^2(A)$ for the ^{56}Fe + ^{56}Fe reaction may be present already in the primary fragment distributions, but it may, as well, be produced by subsequent particle emission. The high excitation energy of fragments from the ^{56}Fe + ^{56}Fe reaction, and, consequently, a comparatively large number of evaporation nucleons, may contribute to this effect. If there is any similar structure present for fragments from the ^{238}U + ^{56}Fe reaction, then it is washed out by the changes in $\bar{Z}$ with E_L (Fig. 3) which are averaged in Fig. 17. Values for $\sigma_Z^2(A)$ that are not averaged over a large range of E_L contain uncertainties too large to draw any conclusions in this reaction.

IV. DISCUSSION

The main properties of the evolution of the *measured* reaction fragment distributions with E_L can be observed simultaneously in Fig. 19. With increasing E_L the distributions become broader in a direction approximately parallel to the line of β stability while keeping their width perpendicular to this direction nearly constant. During this process the distributions rotate in the N-Z plane. Even the *measured* centroids of the distributions (crosses in Fig. 19) show a drift as a function of E_L which is much smaller than the simultaneous increase in width.

The measured properties of the distributions of projectilelike fragments can be compared with predictions from various models. The simplest model, which is also contained as a basis in most more sophisticated calculations, is given by the potential energy surface (PES)

$$V = Q_{gg} + V_c + V_N + V_l , \qquad (9)$$

which takes into account the ground state Q values Q_{gg}, the Coulomb potential V_C, a nuclear potential V_N, and the centrifugal potential V_l. Figure 20 shows examples for
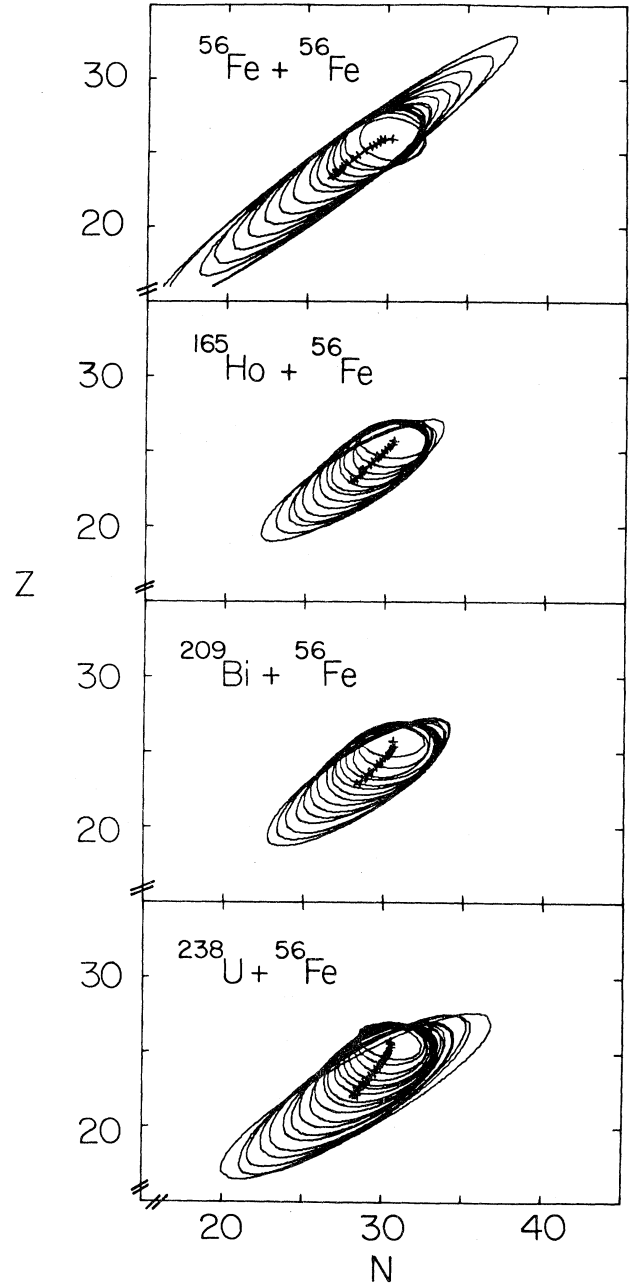

FIG. 19. The contour lines with $P/h = e^{-1/2}$ for the neutron-proton distributions of damped reaction products at several energy losses are shown for the reactions indicated. Starting with the smallest ellipse for each reaction, contour lines are shown for $12 \leq E_L \leq 60$ MeV in 8 MeV steps and for $E_L \geq 60$ MeV in 10 MeV steps. The crosses indicate the centroid of each ellipse. These contour lines represent an overview of the fit results given in Table II to V for the measured (*not* particle-emission corrected) data.

PES calculations with Q_{gg} calculated from the liquid drop mass formula with shell corrections and a suppression of the odd-even effects,[8] and V_N is the proximity potential. The two choices of angular momentum l are for a grazing collision and the minimum angular momentum predicted
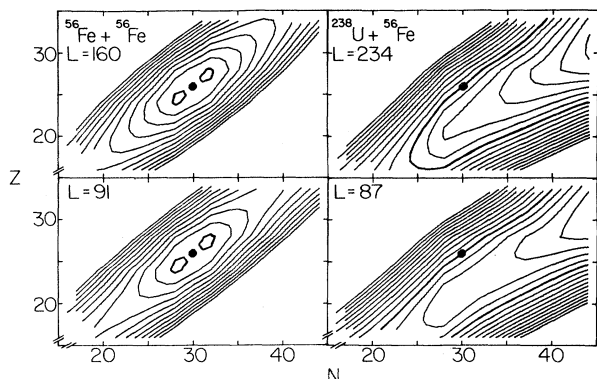
FIG. 20. Potential energy surfaces for the Fe + Fe ($l = 160$ and 91 $\hbar$) and U + Fe ($l = 234$ and 87 $\hbar$) reactions. The calculations include shell corrections and are performed at a target-projectile distance of 8.69 fm for the Fe target and at 11.65 fm for the U target. The potentials are normalized so that $V = 0$ (heavy line) at the injection point ^{56}Fe, which is indicated by circles. The contour lines are 5 MeV apart.

not to lead to fusion.[41] These extreme situations are expected to correspond to quasielastic reactions (small E_L, large l, peripheral reaction, short interaction time) and fully damped reactions (large E_L, smaller l, more central reactions, long interaction times), respectively.

The static model of the PES can be used to estimate the driving forces acting during a considerable portion of the interaction time. The degree of equilibration achieved in the reaction may be defined in terms of the PES. For example, complete charge equilibrations can be defined as the average $\overline{N}/\overline{Z}$ ratio at the local minimum of the PES (Ref. 20) for a given N or Z instead of the N/Z ratio of the combined system,[9] which can only be expected to be reached in a fusion reaction. In a similar way, one may want to define the terms correlated and uncorrelated nucleon exchange. Since a correlation is certainly introduced by the curvature of the PES (and Q_{gg} values incompatible with the energy available at a certain E_L), it may be desirable to separate the correlation effects due to the PES from other correlations possibly present in proton and neutron transfer. However, this has not been possible in this work.

Most dynamical model calculations determine the fate of an average nucleus while interacting with the target and separately calculate the variances for the resulting fragment distributions. Such a treatment may neglect differing dynamical conditions in the many possible exit channels. Projectilelike fragments from an asymmetric reaction which have picked up a large number of nucleons at a certain stage (time) of the interaction may have a much higher probability of being subsequently captured in the fusion or fast fission[39] channel than a light one. The Coulomb barrier, e.g., may inhibit separation sufficiently long to remove the fragment from the projectilelike channel, contrary to a calculation which requires all possible reaction channels to separate simultaneously. These processes and others, such as shell effects only experienced by certain parts of the N-Z distribution, may modify the detected centroids and variances from the ones present

shortly before separation. Similar modifications can be expected for the calculated distributions if the fate of all fragments is determined individually. This could be done rather easily in Monte Carlo (Ref. 27 and references therein) or random walk calculations.[29,30]

A. The centroids of the fragment distributions

The centroids of the *detected* fragment distributions are indicated in Fig. 19. The more quantitative presentations in Figs. 5 and 6, which also give the calculated *primary* $\overline{N}$ values, show that for the three asymmetric reactions (U, Bi, and Ho targets) there is a mass drift towards asymmetry which is nearly exclusively due to proton pickup by the target. Consequently, an increase in the $\overline{N}/\overline{Z}$ ratio is found which is approximately linear with E_L (Fig. 7).

The PES's for the U + Fe reaction in Fig. 20 show that there is a driving force perpendicular to the contour lines from the injection point ($N = 30$, $Z = 26$) towards the valley of the PES. Local minima are found for $N/Z \approx 1.40$ for both the peripheral reactions ($l = 234$) and for rather central collisions ($l = 87$). The corresponding minima in the PES's for the Ho and Bi targets are found at $N/Z \approx 1.30$. These values are reached experimentally at $E_L \approx 130$ MeV for the Ho and Bi targets and at $E_L \approx 180$ MeV for the U target (triangles in Fig. 7). Based on *these* PES's one can conclude that full charge equilibration is achieved only for fully damped reactions. Calculations that allow for changes in separation distance, odd-even effects, and shell effects with excitation energy[20] may, however, yield results which are consistent with full charge equilibration already at earlier stages of the interaction. Recent dynamical calculations that take into account details of the nucleon exchange mechanism[12,27,28,38] have been able to reproduce the experimentally observed $\overline{N}/\overline{Z}$ dependence on E_L quantitatively.[38]

The PES's for all asymmetric reactions predict an increase of more than one neutron and a decrease of more than one proton to reach charge equilibrium (compare Fig. 20). Experimentally, $\overline{N}$ increases by only about 0.6 neutron units for $E_L \lesssim 10$ MeV, and remains constant for higher E_L (Fig. 6), while $\overline{Z}$ decreases (Fig. 5) as expected. The associated experimental mass drift towards more asymmetric mass separation is contrary to all similar PES calculations which predict a drift towards more symmetric fragments in ^{56}Fe-induced reactions. This inconsistency may indicate the importance of dynamical effects during the approach and separation phase of the interaction and the details of the nucleon exchange and energy loss processes, although the aforementioned calculations[12,38] are not yet able to reproduce the measured $\overline{N}$ and $\overline{Z}$ data in Fe-induced asymmetric reactions. The lack of agreement may be partially due to the method of calculating the evolution of an average reaction fragment instead of calculating the mean value of all possible reaction fragments[27] as discussed earlier.

Several experiments[4,5,8] have demonstrated that the charge asymmetry degree of freedom equilibrates much faster than the mass asymmetry degree of freedom, in qualitative agreement with the driving forces given by the PES. For low E_L the modifications of the PES due to the

shell structure of nuclei have also been shown to be important.[10,37] Of special interest is the analysis of the ^{136}Xe + ^{56}Fe reaction at $E_{lab} = 5.9$ MeV/nucleon.[10] In this reaction it was found that (1) the centroids of the damped reaction fragment distributions follow quantitatively the gradient of the PES, and (2) full charge equilibrium is reached after about 40 MeV of E_L. Both observations obtained in the ^{136}Xe + ^{56}Fe reaction contrast with our results. The major differences between these reactions are the larger mass asymmetry and the higher center-of-mass energy $E_{c.m.}$ above the Coulomb barrier E_C per reduced mass μ of the reaction

$$E_R = (E_{c.m.} - E_c)/\mu \qquad (10)$$

in our studies ($E_R = 2.9$ to 5.3 MeV/nucleon) as compared to the Xe + Fe reaction ($E_R \sim 1.9$ MeV/nucleon). This may suggest that only at the lower relative velocity, which is proportional to $E_R^{1/2}$, and/or for low mass asymmetry is the PES sufficient to describe the reaction quantitatively. However, $\bar{Z}$ results obtained for the ^{209}Bi + ^{56}Fe reaction[36] at 6.9 MeV/nucleon ($E_R \approx 1.8$ MeV/nucleon) as well as $\bar{N}$ and $\bar{Z}$ data from the ^{122}Sn + ^{56}Fe reaction[12] at 8.2 and 5.7 MeV/nucleon ($E_R \approx 4.3$ and 1.8 MeV/nucleon, respectively) indicate no dependence of the charge equilibration process on beam energy.

B. The alignment and correlation coefficients of the fragment distributions

For a reaction mechanism that is fully based on statistical nucleon exchange and a hypothetical driving potential V (e.g., a PES) which forms a plane (no curvature) in the N-Z-V frame, one can expect completely uncorrelated neutron and proton exchange. This would result in elliptical contour lines for the fragment distributions in the N-Z plane with the major and minor axis aligned with the N and Z axes. The slope k (defined in Sec. II F) of the major axes with respect to the N axis would be $k = 0$ or $k = \infty$ and the correlation coefficient ρ_{NZ} would vanish. The ratio of the major to minor axes would reflect the ratio of neutrons and protons participating in the exchange process.

Over a small area the PES may be approximated by a tilted plane if odd-even and shell effects are disregarded. Thus, for the very early stages of the reaction (low E_L), where the variances are small (Figs. 10 and 11), ρ_{NZ} and k may be expected to vanish. Therefore, it is not surprising that calculations usually yield vanishing neutron-proton correlation coefficients ρ_{NZ} at low E_L. If the curvature of the PES becomes important (for large variances) the major axis should be aligned with the direction of minimum curvature, and the minor axis with the direction of maximum curvature. Then k would give the slope with respect to the N axis of the direction of minimum curvature which is approximately parallel to the appropriate contour line of the PES. This direction is not necessarily identical with the orientation of the valley of the PES if complete charge equilibration is not reached.

The data (Figs. 9 and 19) show an increase in k at low E_L and nearly constant k above about 40 to 100 MeV of E_L, depending on the reaction. This is in qualitative

agreement with the expectation that, with increasing E_L and total variances, the fragment distributions are increasingly dominated by the curvature of the PES and must consequently also become increasingly correlated with respect to the N-Z coordinates (Fig. 13). The valley of the PES's for the Ho, Bi, and U targets (Fig. 20) all have a slope $k \approx 0.7$ to 0.8. The direction of the contour lines for incompletely charge-equilibrated reaction partners may be even larger. The data show measured slopes of $k \approx 0.70$ and primary slopes of $k' \approx 0.58$ at high E_L in these reactions (Fig. 9). Thus, the data indicate that more neutron-rich heavy nuclei are produced than the PES's predict. Calculations which omit shell effects do not change the results significantly. The measured values of k for the Fe + Fe reaction at high E_L (Fig. 9, $k \approx 0.8$), which can be expected to be close to the primary values, are larger than the slopes of the asymmetric reactions. This is consistent with the larger slope of $k \approx 0.85$ for the PES of this reaction (Fig. 20).

Although we did not find any significant dependence of k on scattering angle, data obtained in the 5.8 MeV/nucleon ^{208}Pb + ^{110}Pd reaction[15] indicate a decrease of k with scattering angle, which possibly accounts for the differences between PES and data. More importantly, however, because of the large variances encountered at these E_L, the data may be particularly sensitive to different *dynamical* conditions at the tails of the distributions, particularly during the exit channel stage of the reaction. This may easily modify the predictions of the *static* PES's.

As the most unexpected result of this investigation, the data show at the lowest E_L ($E_L \leq 15$ to 25 MeV) negative values for k and ρ_{NZ} in all reactions (Figs. 9 and 13). In this E_L region the measured data are not expected to be modified by particle emission due to insufficient excitation energy. Thus they should reflect the primary reaction properties directly. The PES without odd-even and shell effects in conjunction with statistical nucleon exchange does not yield any direct basis for distributions with $k < 0$ and $\rho_{NZ} < 0$. Several additional effects and reaction processes may, however, be responsible for the observed anticorrelation; for example: (1) properties of the data analysis procedure, (2) shell effects, (3) odd-even effects, (4) dynamical effects, (5) charge exchange without nucleon exchange, and (6) vibrations in the charge excess degree of freedom.

An accurate data analysis artificially produces, (1), anticorrelated distributions, if the drift in the N-Z plane is large compared to the variances and if the data are averaged over a large E_L range due to a superposition of many distributions which are offset in the drift direction. However, inspection of Fig. 19 shows that the drift is small compared to the width of the distributions over the energy bins chosen. Analysis of the data with smaller E_L gates reconfirms that the data analysis does not introduce a significant contribution to the values of k and ρ_{NZ}.

Shell effects, (2), do not seem to be strong enough (Fig. 20) to influence the curvature of the PES's near the injection point sufficiently to produce an anticorrelation. Odd-even effects, (3), may be able to channel the nucleon exchange into specific directions, e.g., to favor an ex-

change along $N+Z=$constant, creating an anticorrelation (compare also Sec. III B 2). However, the similarities and systematics in the observed negative k and ρ_{NZ} as a function of the target (Figs. 9 and 13) contrast with the different magnitudes of odd-even effect for the various targets (^{238}U and ^{56}Fe are even-even targets, ^{209}Bi and ^{165}Ho are odd-even targets).

The dynamical conditions in the exit channel, (4), may favor a separation of fragments if the projectile mass is nearly preserved, requiring a minimum of angular momentum transfer. The small variances for σ_A^2 (Refs. 9 and 16; compare also Figs. 10, 11, and 19) do not seem to make dynamical considerations very important at these E_L, however.

A direct statistical charge exchange, (5), without nucleon transfer (e.g., pion exchange[45]) would create distributions that are aligned with $N+Z=$constant and thus result in negative values for k and ρ_{NZ}. Such a process may be important in heavy-ion reactions as demonstrated in a (^{6}Li, ^{6}He) reaction.[45] Anticorrelated distributions could also arise from vibrations, (6), of the neutron against the proton fluid as in isovector giant resonances.[4,23,24,31] Such vibrations would occur along $N+Z=$constant.

The processes (2) to (6), and possibly others, can thus introduce a well-defined anticorrelated component of the distributions along, e.g., $A=$constant. In addition, statistical nucleon exchange is expected to yield approximately constant $k>0$ and correlation coefficients ρ_{NZ} which increase with E_L. Owing to the increasing variances the statistical component can be expected to dominate the distributions for large E_L if the other component does not increase in variance along $A=$constant. Thus, the data showing a continuous increase of k and ρ_{NZ} with E_L from negative values at the lowest E_L are not inconsistent with the superposition of distributions arising from two separate processes.

No data published[6,10,12,13,19,22] so far by other groups exhibit conclusive evidence for negative k or ρ_{NZ}. However, those data are not necessarily incompatible with our observations. As is evident from the data presented, a very detailed analysis is necessary to observe these effects. Larger bins in E_L than the ones used in this paper (± 2 MeV) combined with the usually larger statistical uncertainties can easily mask these features. In fact, new high resolution data obtained by our group (Rochester-Indiana-Maryland collaboration) for the ^{238}U + ^{40}Ca reaction[18] with excellent statistical significance again confirm the presence of negative k and ρ_{NZ} at the lowest E_L.

At present, no calculations have been published which show negative k and ρ_{NZ} (Refs. 12, 31, 38, and 44). These calculations do not include, however, details of the processes (2) to (6) and of direct reactions which could be important, maybe even dominant, at low E_L. Calculations which consider collective vibrations in the charge excess degree of freedom[4,7,23,24,31] have not yet been used to predict k or ρ_{NZ}. Random walk calculations[29,30] possibly can take the properties of individual nuclei, e.g., odd-even effects, into account most easily.

The correlation coefficient ρ_{NZ} is a very sensitive indicator of the early stages of the reaction (at low E_L) since it contains elements of σ_Z^2, σ_N^2, and k. Thus, in order for a

calculation to reproduce the measured ρ_{NZ} at low E_L, all direct statistical energy loss processes, as well as the structure of the nuclei involved should be considered. At high E_L, ρ_{NZ} is a less sensitive measure of the reaction. Here, ρ_{NZ} is dominated by the large variances and may in addition be sensitive to distortions due to particle decay if both neutron *and* proton emission are possible.[44] However, *pure* neutron evaporation leaves ρ_{NZ} nearly unchanged. With decreasing E_L and increasing target mass the importance of particle decay decreases. Thus, the ^{238}U + ^{56}Fe reaction should give the best approximation of the ρ_{NZ} values of the primary reaction products over the full E_L range and should be used primarily for a comparison with future theoretical calculations.

C. The total variances of the fragment distributions

The total variances for the proton and neutron distributions, σ_Z^2 and σ_N^2 (Figs. 10 and 11), and also for the mass distributions,[9,16] σ_A^2, are in qualitative agreement with results from many other low energy heavy-ion studies. The increase in the variances with E_L is expected theoretically if statistical nucleon exchange is an important process for energy dissipation. The correlation coefficients ρ_{NZ} and ρ_{AZ} in Fig. 13 demonstrate that this proton and neutron exchange cannot proceed completely independently.

The detection of fragments with energies less than the mutual Coulomb energies for peripheral nuclei (arrows in Figs. 10 and 11) signifies that at high E_L the interaction partners are strongly deformed. This is most apparent for the ^{238}U + ^{56}Fe reaction.

Variances for the ^{58,64}Ni, ^{122}Sn + ^{56}Fe reactions at 8.2 MeV nucleon can be extracted from the data in Ref. 12. The values of σ_N^2 and σ_Z^2 for the Sn target are very similar to our data for the asymmetric reactions. The variances for the ^{58,64}Ni targets are slightly smaller than those for the Fe + Fe reaction.

Note that for the Fe + Fe reaction the variances σ_Z^2 and, less pronounced, σ_N^2 are significantly larger than those of the asymmetric reactions. If σ_Z^2 and σ_N^2 reflect the number of protons and neutrons, respectively, exchanged in the energy loss process, then increased variances for the Fe + Fe reaction can be expected on the basis of the narrower valley of the PES as compared to the asymmetric reactions: fewer nuclei are accessible in the valley for constant A. Thus, the distributions are forced to evolve more strongly along the valley. Actually, the variances for the Fe + Fe reaction should be most easily reproduced, since additional features have to be considered for the asymmetric reactions. Such features are, e.g., (1) the lower excitation energies per nucleon at a given E_L and consequently larger importance of properties of individual nuclei, (2) possible correlations between charge equilibration process and particle diffusion, and (3) the fact that the high and low Z tails of the distributions are not equivalent, as they are in the Fe + Fe reaction. The similarity of the ^{56}Fe + ^{56}Fe and ^{58,64}Ni + ^{56}Fe data[12] indicates that features related to the projectile-target mass asymmetry are most important for the changes of the variances with the target nucleus.

Within the experimental uncertainties the ratio of the

neutron-to-proton variances σ_N^2/σ_Z^2 (Fig. 12) is approximately constant for $E_L \geq 30$ MeV. At low E_L, however, all asymmetric reactions, and possibly also the Fe + Fe reaction, show a marked increase in σ_N^2/σ_Z^2. These enhanced ratios are mainly a consequence of the initial strong increase of σ_N^2 below $E_L \approx 10$ MeV (Fig. 11), rather than small σ_Z^2 values. These results are confirmed by similar data from ^{56}Fe-induced reactions with ^{58,64}Ni and ^{122}Sn targets.[12] Ground-state Q-value effects do not appear to be strong enough to explain the enhanced neutron variances in these reactions. Angular momentum mismatch (lower relative energy balanced by higher average mass) in conjunction with charge equilibration may favor enhanced neutron transfer in the asymmetric reactions.

Some other experiments[5,6,8,31] performed with heavier projectile-target combinations have shown more dramatic increases in σ_N^2/σ_Z^2 or σ_A^2/σ_Z^2 ratios for the early stages of the interaction. (Note that increased σ_N^2/σ_Z^2 ratios do *not* necessarily imply increased σ_A^2/σ_Z^2 values.[2,16]) These observations have been interpreted in terms of a neutron skin around the interacting nuclei[38] (induced or initially present) or an inhibition of proton exchange due to Coulomb effects[31,32] in the early stages of the interaction. Theoretical calculations[31,38] can account to a certain degree for the experimentally observed ratios of total variances.

D. The variances for fixed neutron, proton, and mass number

For a two-dimensional Gaussian distribution, any variance along a certain axis (e.g., fixed A, N, or Z) is identical to any other variance along any parallel axis. Thus, the variances at constant N, Z, and A represent the cross-section—averaged variances for all possible constant, N, Z, and A. The variances at fixed A, $\sigma_Z^2(A) = \sigma_N^2(A)$, are related to the flux of protons and neutrons between the colliding nuclei. This is suggestive of isovector vibrations. The variances at fixed neutron number, $\sigma_Z^2(N) = \sigma_A^2(N)$, and at fixed proton number, $\sigma_N^2(Z) = \sigma_A^2(Z)$, in contrast, may yield information on the *in*dependence of proton and neutron exchange between projectile and target. However, before these properties can be extracted, the stringent limitations imposed on such variances due to energy conservation (Q_{gg}) and, less stringent, the PES, must be considered (Fig. 20). Cuts through the PES along constant A, Z, and N are roughly parabolic. Thus, the PES requires upper limits for the variances which vary approximately proportional to $E_L^{1/2}$, with the smallest values for $\sigma_Z^2(A)$ and the largest for $\sigma_N^2(Z)$ at a given E_L. Since the asymmetric reactions do not originate from a local minimum of the PES, one may expect a more rapid increase in the variances at low E_L than predicted by $E_L^{1/2}$.

The relative magnitudes of the experimental variances, $\sigma_Z^2(N)$, $\sigma_N^2(Z)$, and $\sigma_Z^2(A)$ behave qualitatively as expected (Figs. 14—16). The values of the variances at high E_L increase with target mass in agreement with the width of the PES's (Fig. 20). However, the data show the following features which are of special interest.

(a) Much smaller variances than the upper limits given by the PES's are observed [e.g., for the Fe + Fe reaction $\sigma_Z^2(A) \approx 3$ for $E_L = 20$ MeV and $\sigma_Z^2(A) \approx 5.5$ for $E_L = 50$ MeV are allowed; values < 1.0 are measured].

(b) The variances are consistent with constant values above certain E_L ("plateau"); this is most pronouced for $\sigma_Z^2(A)$.

(c) The rate of increase of all variances with E_L is fastest for the symmetric reaction and decreases systematically as a function of increasing mass symmetry.

Thus, other factors than the simple PES limitations must be of importance for the experimentally observed variances shown in Figs. 14—16. One of these factors may be particle evaporation of the excited primary fragments. Evaporation may modify the primary variances[12,18,44] significantly, especially if one assumes them to be much larger than the measured variances and if both neutron *and* proton evaporation are present. Primary variances for $\sigma_Z^2(A)$ much larger than 1.0, however, seem to be incompatible[18] with the measured data shown in Fig. 16.

As observed in Figs. 14—16, the amount of E_L necessary to reach a plateau in these variances appears to be related to the total mass or charge of the system. This is most suggestive for $\sigma_Z^2(A)$. Assuming thermal equilibrium during all stages of the interaction, this may indicate that a minimum nuclear temperature T or projectilelike fragment excitation energy E^* is necessary to obtain a final constant variance. For $\sigma_Z^2(A)$ this would be $E^* \approx 10$ MeV or $T \approx 1.2$ MeV. For $\sigma_Z^2(N)$ and $\sigma_N^2(Z)$ one would obtain $E^* \approx 15$ MeV or $T \approx 1.5$ MeV. The observation that these excitation energies correspond approximately to the neutron and proton evaporation threshold, respectively, in a projectilelike fragment may have some influence on the observed variances.

Experimental data for variances at constant A, N, or Z have been published for a few additional reactions (Refs. 3—7, 12, and 18). Although the absolute magnitude of the variances are not necessarily always comparable[1,2,16] due to different analysis techniques and corrections for experimental resolution,[1,2,16] the general properties of the variances from these data are expected to be little affected. The general trend seen is a rapid increase in $\sigma_Z^2(A)$ within about the first 50 MeV of E_L. The results for $\sigma_Z^2(A)$ derived from several reactions [^{40}Ca + ^{37}Cl, ^{209}Bi + ^{37}Cl, and ^{238}U + ^{40}Ca (Ref. 18), ^{86}Kr + ^{92,98}Mo (Ref. 4), ^{208}Pb + ^{94}Zr, and ^{208}Pb + ^{110}Pd (Refs. 3 and 5), and possibly ^{58,64}Ni + ^{56}Fe, and ^{122}Sn + ^{56}Fe (Ref. 12)] consistently show a plateau for high E_L, in agreement with results from our data for ^{56}Fe-induced reactions (Fig. 16, Refs. 1, 2, and 16). In contrast, radiochemical studies of the ^{132}Xe + ^{197}Au reaction,[6,7] the heaviest system for which $\sigma_Z^2(A)$ values have been published, show continuously increasing variances as a function of E_L. The beam energy of 6.8 MeV/nucleon for the latter reaction lies well within the range of beam energies in the former studies (5.0 to 8.3 MeV/nucleon), as well as the relative velocities of reaction partners [$E_R \approx 0.9$ to 5.3; compare Eq. (10)]. Thus, a simple beam energy or relative velocity dependence of the saturation of $\sigma_Z^2(A)$ can be excluded. Since pure neutron evaporation is not expected to produce a plateau in the measured distributions, the variety of projectile target

combinations and beam energies used indicates that a plateau for $\sigma_Z^2(A)$ values exist in many reactions, possibly along with a continuously increasing $\sigma_Z^2(A)$ for much heavier systems[6,7] like ^{132}Xe + ^{197}Au. The latter is not inconsistent with a systematic increase in the E_L required to reach the plateau (Fig. 16) with the *product* of the masses or charges of projectile and target, although it contradicts the mentioned correlation with nuclear temperature or fragment excitation energy.

Several calculations have been performed that emphasize the charge excess degree of freedom to account for the observed variances $\sigma_Z^2(A)$. Constant variances are expected if collective processes with an eigenenergy $\hbar\omega$ that is large compared to the nuclear temperature T are responsible for the observed variances[4,23,24,31] (quantal fluctuations). This applies, e.g., to the isovector giant dipole resonance ($\hbar\omega \approx 10$ MeV, $T \lesssim 3$ MeV). Most data, including those[1] of the ^{56}Fe-induced reactions, are in agreement with calculations based on quantal fluctuations. For $\hbar\omega \lesssim T$ statistical effects dominate[6,7,31] and the shape of the PES together with level density arguments allows for an increase of $\sigma_Z^2(A) \propto T$, which is approximately proportional to $E_L^{1/2}$ (statistical fluctuations). The ^{132}Xe + ^{197}Au data compare favorably with the latter calculations. The measured variances at fixed A, N, and Z are also consistent with the results of random walk calculations, where the approximation of the PES by a "slot"[29] yields excellent agreement with the measured $\sigma_Z^2(A)$ while using the actual parabolic PES results[30] in continuously increasing $\sigma_Z^2(A)$. Other calculations, which do not invoke modes with large $\hbar\omega$, but take into account Pauli blocking, also give rather good agreement with the experimental data.[12,38]

V. CONCLUSIONS

In this paper we have presented a systematic experimental study of the mass and charge distributions of projectilelike fragments observed in ^{56}Fe-induced reactions at about 140 MeV above the entrance channel Coulomb barrier. The data have been parametrized in terms of a two-dimensional Gaussian function. This provides a small set of E_L-dependent parameters which can be used to calculate specific quantities of interest for comparison with theoretical calculations and other published data. The properties of the fragment distributions in the N-Z plane can be generally accounted for by these parameters, although fine structure in the data requires more detailed analysis. The results given in the tables are fit results for the experimentally observed distributions, corrected for the known artifacts due to experimental resolution and the fitting procedure. Although we also present calculated primary data in the figures, we believe that reliable evaporation calculations should be applied to the results from model calculations where, in principle, all quantities are known. This has been done in some cases.[12,24,44] If a direct comparison between theoretical calculations and experimental data is desired, the ^{238}U + ^{56}Fe reaction should be considered first, since particle decay is least important

here. It is worthwhile to remember that, among the properties discussed, the variances at fixed A, N, and Z numbers may be most strongly affected by particle evaporation and that its influence increases with E_L.

Data that provide not only the charge of individual damped fragments, but also their masses with good resolution, provide a much more detailed view of the reaction mechanism. Notably, the neutron-proton correlation coefficient ρ_{NZ} and the variance at constant A, N, and Z emphasize the restrictions imposed on the independent diffusion of protons and neutrons between the reaction partners by the potential energy surface PES. However, the data and calculations indicate that additional properties of nuclear matter may influence the energy damping process over the full range of E_L, e.g., the Pauli principle, fixed particle-hole densities, pion exchange, or high frequency vibrations. Deformations of the interaction partners, as suggested by the projectilelike fragments detected at very high E_L, are another ingredient to be accounted for in most dynamical calculations.

While the PES's calculated for these data provide a rather good qualitative prediction of the evolution of fragment distributions in the N-Z plane, a quantitative agreement is not obtained, especially at low E_L. The path of the average proton and neutron number does not follow exactly the gradient of the PES, and the PES gives no direct suggestions about the origin of N-Z distributions that are anticorrelated with respect to the N-Z frame. The dynamical changes of the interaction potential are almost certainly of great importance at these low E_L values, where the interaction partners presumably remain only a very short time in a nearly static potential. The negative correlation coefficients suggest strongly that nonstatistical energy loss processes are present and/or that the detailed properties of *individual* nuclei are of dominant importance in addition to a statistical nucleon exchange.

The data represent a detailed and high precision description of a subset of damped heavy-ion reactions. They establish stringent conditions for any kind of theoretical calculations that can be compared with such data. The choice of several different targets with a wide range of neutron-excess and mass-symmetry values demonstrates the systematic trends of the interaction observables. In addition, it provides confidence that the properties investigated are not specific to only one certain heavy-ion reaction. The comparison with other available data confirms these conclusions.

A quantitative comparison of variance-related data from different experimental studies rests to a certain degree on the analysis procedure used.[16] In addition, it is apparent that high statistical accuracy is required to obtain detailed results, such as the negative ρ_{NZ} at low E_L. Also, excellent experimental mass and charge resolution is mandatory to obtain precise values for all centroids and variances. Both requirements usually result in the need for large amounts of beam time due to the fourfold differential cross section $d^4\sigma/dE\,d\theta\,dA\,dZ$. To extend the data base given by the reaction discussed, it is desirable to change both the energy available for dissipation as well as the type of projectile systematically in subsequent experiments. These projects are currently in progress.

ACKNOWLEDGMENTS

*Present address: Cyclotron Institute, Texas A&M University, College Station, TX 77843.

†Present address: Hahn-Meitner Institut, Glienicker Strasse 100, D-1000 Berlin 39, Federal Republic of Germany.

[1] A. C. Mignerey, V. E. Viola, Jr., H. Breuer, K. L Wolf, B. G. Glagola, J. R. Birkelund, D. Hilscher, J. R. Huizenga, W. U. Schröder, and W. W. Wilcke, Phys. Rev. Lett. 45, 509 (1980).

[2] H. Breuer, A. C. Mignerey, V. E. Viola, K. L. Wolf, J. R. Birkelund, D. Hilscher, J. R. Huizenga, W. U. Schröder, and W. W. Wilcke, in the Proceedings of the IXth International Workshop on Gross Properties of Nuclei and Nuclear Excitations, Hirschegg, Austria, 1981, p. 162.

[3] K. H. Rehm, E. Essel, K. Hartel, P. Kienle, H. J. Körner, R. E. Segel, P. Speer, and W. Wagner, Z. Phys. A 293, 119 (1979).

[4] M. Berlanger, A. Gobbi, F. Hanappe, U. Lynen, C. Ngô, A. Olmi, H. Sann, H. Stelzer, H. Richel, and M. F. Rivet, Z. Phys. A 291, 133 (1979).

[5] K. E. Rehm, H. Essel, P. Sperr, K. Hartel, P. Kienle, H. J. Körner, R. E. Segel, and W. Wagner, Nucl. Phys. A366, 477 (1981).

[6] J. V. Kratz, J. Poitou, W. Brüchle, H. Gäggeler, M. Schädel, G. Wirth, and R. Lucas, Nucl. Phys. A357, 437 (1981).

[7] J. Poitou, R. Lucas, J. V. Kratz, W. Brüchle, H. Gäggeler, M. Schädel, and G. Wirth, Phys. Lett. 88B, 69 (1979).

[8] J. V. Kratz, W. Brüchle, G. Franz, M. Schädl, I. Warnecke, and G. Wirth, Nucl. Phys. A332, 477 (1979).

[9] H. Breuer, B. G. Glagola, V. E. Viola, K. L. Wolf, A. C. Mignerey, J. R. Birkelund, D. Hilscher, A. D. Hoover, J. R. Huizenga, W. U. Schröder, and W. W. Wilcke, Phys. Rev. Lett. 43, 191 (1979).

[10] D. Schüll, W. C. Shen, H. Freiesleben, R. Bock, F. Busch, D. Bangert, W. Pfeffer, and F. Pühlhofer, Phys. Lett. 102B, 116 (1981).

[11] Y. Eyal, G. Rudolf, I. Rode, and H. Stelzer, Phys. Rev. Lett. 42, 826 (1979).

[12] H. C. Britt, B. H. Erkkila, A. Gavron, Y. Patin, R. H. Stokes, M. P. Webb, P. R. Christensen, Ole Hansen, S. Pontoppidan, F. Videbaek, R. L. Ferguson, F. Plasil, G. R. Young, and J. Randrup, Phys. Rev. C 26, 1999 (1982).

[13] E. C. Wu, K. D. Hildenbrand, H. Freiesleben, A. Gobbi, A. Olmi, H. Sann, and U. Lynen, Phys. Rev. Lett. 47, 1874 (1981).

[14] H. Essel, K. Hartel, W. Henning, P. Kienle, H. J. Körner, K. E. Rehm, P. Sperr, W. Wagner, and H. Spieler, Z. Phys. A 289, 265 (1979).

[15] H. Essel, K. Hartel, P. Kienle, H. J. Körner, K. E. Rehm, P. Sperr, and W. Wagner, Phys. Lett. 81B, 161 (1979).

[16] H. Breuer, N. R. Yoder, A. C. Mignerey, V. E. Viola, K. Kwiatkowski, and K. L. Wolf, Nucl. Instrum. Methods 204, 419 (1983).

[17] H. Breuer, K. L. Wolf, B. G. Glagola, K. Kwiatkowski, A. C. Mignerey, V. E. Viola, W. W. Wilcke, W. U. Schröder, J. R. Huizenga, D. Hilscher, and J. Birkelund, Phys. Rev. C 22, 2454 (1980).

[18] A. C. Mignerey, H. Breuer, K. L. Wolf, R. R. Betts, C. Davids, B. G. Glagola, and V. E. Viola, in the Proceedings of the International Summer School Mikolajki, Poland, 1981; A. C. Mignerey et al., University of Maryland Nuclear Chemistry Progress Report No. ORO-5172-0020, 1982, p. 2; H. Breuer et al., ibid. p. 16; A. C. Mignerey et al., ibid., p. 31.

[19] T. H. Chiang, D. Guerreau, P. Auger, J. Galin, B. Gatty, X. Tarrago, and J. Girard, Phys. Rev. C 20, 1408 (1979).

[20] J. V. Kratz, W. Brüchle, H. Gäggeler, M. Schädel, K. Sümmerer, and G. Wirth, Z. Phys. A 296, 141 (1980).

[21] M. F. Rivet, R. Bimbot, D. Gardès, G. Mouchaty, A. Fleury, F. Hubert, and Y. Llabador, Z. Phys. A 296, 201 (1980).

[22] B. Gatty, D. Guerreau, M. Lefort, X. Tarrago, J. Galin, B. Cauvin, J. Girand, and H. Nifenecker, Nucl. Phys. A253, 511 (1975).

[23] E. S. Hernandez, W. D. Myers, J. Randrup, and B. Remaud, Nucl. Phys. A361, 483 (1981).

[24] H. Hofmann, C. Grégoire, R. Lucas, and C. Ngô, Z. Phys. A 293, 229 (1979).

[25] L. G. Moretto, J. Sventek, and G. Mantzouranis, Phys. Rev. Lett. 42, 562 (1979).

[26] L. G. Moretto, C. R. Albiston, and G. Mantzouranis, Phys. Rev. Lett. 44, 924 (1980).

[27] J. Randrup, Nucl. Phys. A327, 490 (1979).

[28] W. U. Schröder, J. R. Birkelund, J. R. Huizenga, W. W. Wilcke, and J. Randup, Phys. Rev. Lett. 44, 308 (1980).

[29] J. J. Griffin, Y. Boneh, K. K. Kan, and M. Dworzecka, Nucl. Phys. A369, 181 (1981).

[30] J. J. Griffin, Y. Boneh, M. Dworzecka, and K. K. Kan, Nucl. Phys. A382, 159 (1982).

[31] D. H. E. Gross and K. M. Hartman, Phys. Rev. C 24, 2526 (1981).

[32] U. Brosa and D. H. E. Gross, Z. Phys. A 298, 91 (1980).

[33] S. S. Kapoor and J. N. Dee, Phys. Rev. C 26, 173 (1982).

[34] D. Hilscher, J. R. Birkelund, A. D. Hoover, W. U. Schröder, W. W. Wilcke, J. R. Huizenga, A. C. Mignerey, K. L. Wolf, H. F. Breuer, and V. E. Viola, Jr., Phys. Rev. C 20, 576 (1979).

[35] A. D. Hoover, J. R. Birkelund, D. Hilscher, W. U. Schröder, W. W. Wilcke, J. R. Huizenga, H. Breuer, A. C. Mignerey, V. E. Viola, Jr., and K. L. Wolf, Phys. Rev. C 25, 256 (1982).

[36] H. Breuer et al., University of Maryland Nuclear Chemistry Progress Report No. ORO-5172-11, 1978, p. 4; H. Breuer et al., University of Maryland Nuclear Chemistry Progress Report No. ORO-5172-14, 1979, p. 14.

[37] M. Dakowski, A. Gobbi, and W. Nörenberg, Nucl. Phys. A378, 189 (1982).

[38] W. U. Schröder, J. R. Huizenga, and J. Randrup, Phys. Lett. 98B, 355 (1981); W. U. Schröder, private communication.

[39]V. Bernard, C. Grégoire, C. Mazur, C. Ngô, M. Ribrag, G. Y. Fau, P. Gonthier, H. Ho, W. Kühn, and J. P. Wurm, Nucl. Phys. <u>A385</u>, 319 (1982), and references therein.

[40]I. S. Sherman, R. G. Roddick, and A. F. Metz, IEEE Trans. Nucl. Sci. <u>15</u>, 500 (1968).

[41]W. W. Wilcke, J. R. Birkelund, H. J. Wollersheim, A. D. Hoover, J. R. Huizenga, W. U. Schröder, and L. E. Tubbs, At. Data Nucl. Data Tables <u>25</u>, 391 (1980).

[42]P. Belery, T. Delbar, and G. Grégoire, Nucl. Instrum. Methods <u>179</u>, 1 (1981).

[43]A. H. Wapstra and K. Bos, At. Data Nucl. Data Tables <u>19</u>, 177 (1977).

[44]D.-K. Lock, R. Vandenbosch, and A. Lazzarini, Nucl. Phys. <u>A384</u>, 241 (1982).

[45]G. Ciangaru, Nucl. Phys. <u>A398</u>, 371 (1983).